PHILOSOPHICAL MAGAZINE A, 2002, VOL. 82, NO. 3, 429–462

Taylor & Francis
Taylor & Francis Group

Numerical modelling of martensitic growth in an elastoplastic material

VALERY I. LEVITAS†, ALEXANDER V. IDESMAN

Texas Tech University, Department of Mechanical Engineering, Lubbock, Texas 79409-1021, USA

GREGORY B. OLSON

Department of Materials Science and Engineering, Northwestern University, 2225 North Campus Drive, Evanston, Illinois 60208-3108, USA

and ERWIN STEIN

Institute of Structural and Computational Mechanics, University of Hannover, Appelstrasse 9A, 30167 Hannover, Germany

[*Received 8 January 2001 and accepted in revised form 13 June 2001*]

ABSTRACT

A finite-strain-continuum thermomechanical approach is applied to the problem of temperature-induced martensitic transformation in elastoplastic materials. The key issue is to determine the transformation-induced stress and plastic strain fields and their effect on the thermodynamics and kinetics of transformation. The problems of appearance and growth of a temperature-induced rectangular martensitic unit in an austenitic matrix in both bulk and near-free-surface environments are formulated, solved and analysed. Very complex and heterogeneous stress–strain fields in the austenite and martensite phases and their non-monotonic time variation are predicted. Plastic shear strain at some points can reach 60% and, after an elastic growth stage, change sign and vary by 40%. The interface velocity as a function of temperature and interface position is calculated. After the appearance of a martensitic particle, transformation work, which is the only variable part of the interface driving force, decreases by a factor of two during lengthening of the particle by 10%. The component of the athermal interfacial friction due to dislocation forest hardening increases significantly as well, leading to interface deceleration and growth arrest. A free surface does not significantly affect the driving force until its distance from the moving interface falls below 0.75 times the particle thickness. Then the transformation work increases while the accumulated plastic strain and associated dislocation forest hardening decrease sharply. If the interface is not arrested at this point, it then accelerates to the free surface where an asymmetric plastic zone leaves 'tent-shaped' surface relief. The motion of a small step at the martensitic plate interface is studied as well. In contrast with elastic growth, the thermodynamic conditions for lengthening and thickening are almost equivalent for plastic growth. The results obtained allowed us to address the following fundamental problems: firstly, the morphological transition from plate to lath martensite; secondly, the relation of thermally activated kinetics at the interface level to athermal kinetics at the macrolevel; thirdly, the concentration of

† Email: valery.levitas@coe.ttu.edu

Philosophical Magazine A ISSN 0141–8610 print/ISSN 1460-6992 online
http://www.tandf.co.uk/journals
DOI: 10.1080/01418610110075483

dislocations and plastic strain in martensite rather than in austenite despite the much higher yield stress of martensite in comparison with austenite.

§ 1. Introduction

Martensitic phase transformation in steels is characterized by a combination of 2–5% volumetric transformation strain and 20% transformation shear. The appearance of such high eigenstrains in martensitic regions is known to be accompanied by plastic deformation (accommodation) in the austenite and martensite. Figure 1 shows a typical lath martensitic microstructure in a quenched alloy steel (commercial

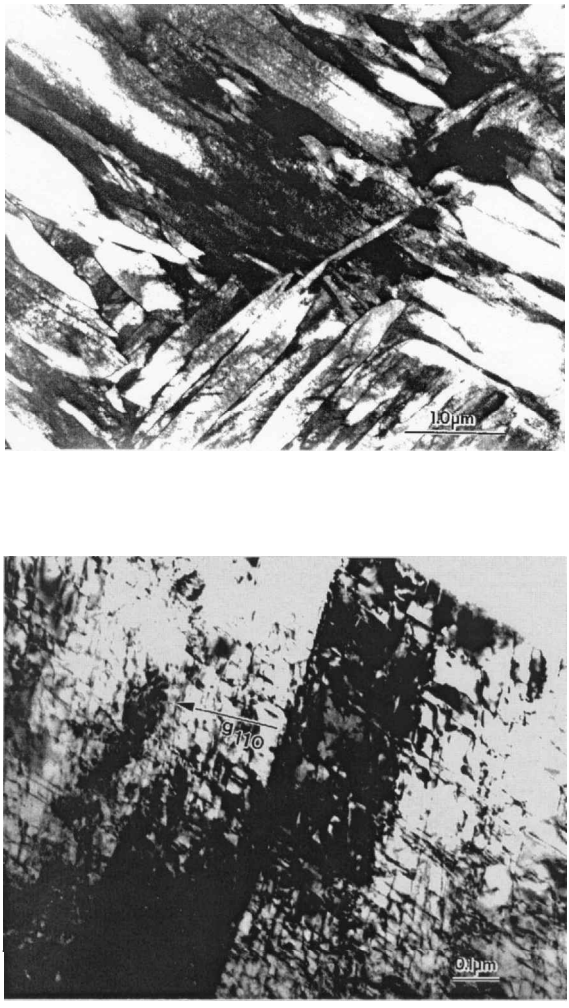

Figure 1. (*a*) Bright-field transmission electron micrograph of lath martensite microstructure in Ferrium C69 steel oil quenched from 1100°C (courtesy of Dr Gautam Ghosh). (*b*) Higher-magnification view showing the dislocation substructure associated with plastic accommodation during martensitic growth (courtesy of Dr Gautam Ghosh).

Ferrium C69 steel Fe–28 wt% Co–3 wt% Ni–5 wt% Cr–2.5 wt% Mo–0.17 wt% C marketed by QuesTek Innovations) with a high transformation temperature. The higher magnification view in figure 1(*b*) shows the dislocation substructure within the laths associated with plastic accommodation during growth. This plastic deformation changes the stress field, driving force and kinetics of martensitic transformations. It has been proposed that plastic accommodation causes the technologically important plate–lath morphological transition in steels (Olson and Cohen 1986, Haezebrouck 1987).

Plate martensite grows radially until it is stopped by a strong inhomogeneity, such as a grain boundary or other martensite plate. Lath martensite is arrested inside the grain without any such inhomogeneity. The problem is to find a mechanism for the growth arrest, which will identify material parameters controlling the plate–lath morphological transition and microstructure. Another problem is to explain why dislocations and consequently plastic strain are concentrated in martensite rather than in austenite despite the fact that the yield stress of martensite is three times the yield stress of austenite. A further question is the exact relation between thermally activated kinetics at the interface level and athermal kinetics at the macrolevel.

Owing to the complexity of interactions, a reasonable approach to these problems is to develop a proper thermomechanical model and to study the martensite growth numerically. This will reveal stress and plastic strain fields due to the martensitic phase transformation (PT), to separate and estimate the effect of each contribution (stress and plastic strain) on the driving force for and on the resistance to interface propagation.

The first model of martensitic plate growth in the plastic regime (Olson and Cohen 1986, Haezebrouck 1987), despite a very approximate treatment of stress–strain fields, revealed some very important features, in particular longitudinal growth arrest due to plastic accommodation. The first finite-element study of the appearance and thickening of a martensitic plate with fixed ends (Marketz and Fischer 1994a,b) employed a small strain formulation. However, as will be shown here, this is far from reality, because plastic shear reaches 0.6. To predict the progress of transformation a criterion of maximum transformation work (Patel and Cohen 1953), $\boldsymbol{\sigma} : \boldsymbol{\varepsilon}_t$, is employed where $\boldsymbol{\varepsilon}_t$ is the transformation strain tensor and $\boldsymbol{\sigma}$ is the stress tensor in a transforming element before PT. As shown by Levitas (1997, 1998a,b), a principle of maximum actual transformation work with allowance for stress variation in the transforming region has to be used, which differs significantly from $\boldsymbol{\sigma} : \boldsymbol{\varepsilon}_t$ and can even have opposite sign (Levitas *et al.* 1998).

In the paper by Wen *et al.* (1999) a small-strain finite-element solution was obtained for modelling the growth by discrete martensitic layers. Transformation in each layer was modelled by homogeneous growth of the transformation strain from zero to its final value. A PT criterion and an extremum principle to choose the next transforming layer were proposed which differ from those derived thermodynamically (Levitas 1997, 1998a,b). Kinetic equations were not employed in the above papers by Marketz and Fischer (1994a,b) and Wen *et al.* (1999).

Recently a mesoscopic continuum thermomechanical theory of martensitic PT in inelastic materials has been developed at both small and finite strains (see Levitas (1997, 1998a, 2000), and references herein) and applied to analytical (Levitas 1997, 1998a, 2000) and numerical solutions of a number of model problems (Levitas *et al.* 1998, 1999, Idesman *et al.* 1997, 1999, 2000). It appears that a number of experimental results related to the interaction of plastic strain and PT can be explained,

based on this theory and the solutions obtained; in particular, for martensite nucleation at shear-band intersections for strain-induced PT (Levitas *et al.* 1999) and PT under compression and shear of materials in Bridgman anvils (Levitas 1997).

To illustrate the numerical algorithms developed (Idesman *et al.* 1999), a problem of the appearance of a martensitic plate in an elastoplastic austenitic matrix was solved at finite strains based on this theory. The thermodynamic driving force for the appearance of plates with different ratios l/h of the length l to the thickness h of the plate was calculated. However, a detailed analysis of stress–strain fields was not made. It was determined that, the larger the aspect ratio l/h, the larger is the driving force for the PT, but the dependence is nonlinear.

The longitudinal 'growth' of a plate with the initial aspect ratio $l/h = 2$ was treated in the paper by Idesman *et al.* (1999) as the sequential appearance of a next plate with $l/h = 2$ contacting the previous plate. It was determined that the driving force does not change during this type of 'growth' process. Consequently, stable plate growth occurs, which can only be stopped at a strong heterogeneity such as a grain boundary. However, such a process does not correspond to the actual process of continuous interface propagation through the plastically deformed matrix, because the length of each new unit in which transformation strain increases homogeneously from zero to its final value, exceeds by a factor of two the size of plastic zone induced by PT in the previous unit. Thus the driving force for the appearance of the first plate in undeformed material and for each next unit is the same, that is the solution does not feel the effect of a small plastic zone.

The aims of the present paper are as follows:

(i) to formulate a complete system of equations describing the plastic growth of a martensitic particle in an austenitic matrix allowing for coupling between the PT and stress and plastic strain fields, as well as for finite strains;
(ii) to study in detail the variation in the stress–strain fields caused by the transformation process, while taking into account the plastic strain in austenite inherited by growing martensite; also, to estimate the validity of simplified stress–strain fields used in previous literature;
(iii) to investigate the effect of stress–strain fields on the thermodynamic driving force for interface propagation, the athermal resistance to interface motion and the resulting interface velocity;
(iv) to apply the results to fundamental problems of the lath–plate morphological transition in steels and the relation of thermally activated kinetics at the interface level to athermal kinetics at the macrolevel; also, to explain why dislocations and plastic strain are concentrated in martensite rather than in austenite despite the fact that the yield stress of martensite is three times the yield stress of austenite.

All calculations will be made for three cases: growth of a martensitic unit inside the bulk austenite, growth of a martensite unit near a free surface, and the appearance and growth of a small step at the martensitic plate interface.

In § 2 a problem formulation for the martensitic PT in elastoplastic isotropic materials at finite strains is presented. We consider finite plastic and transformation strains and small elastic deformations. A complete set of constitutive equations, transformation criteria and the kinetic equation as well as the extremum principle for the determination of the location and volume of transformed increments are presented. The interface propagation criterion and kinetic equation suggested in

this paper combine the advantage of strict continuum thermodynamic derivation of the expression for the driving force $\bar{X}$ with a physically based equation for athermal and thermal parts of the interfacial friction obtained in Olson and Cohen (1986), Ghosh and Olson (1994) and Levitas (1998a,b).

The basic features of the numerical algorithm developed (see also the paper by Idesman *et al.* (1999)) are included in § 3. Based on the finite-element method (FEM) the numerical approach allows us effectively to study very complicated physically and geometrically nonlinear problems.

In § 4.1 the problem of the appearance and growth of a temperature-induced martensitic unit in an austenitic matrix is formulated, solved and analysed. Very complex and heterogeneous stress–strain fields in austenite and martensite and their non-monotonic time variation are obtained. Plastic shear strain at some points can reach 60% and, after an elastic stage, change sign and vary by 40%. After the appearance of the martensitic unit, transformation work, which is the only variable part of the interface driving force, decreases by a factor of two during lengthening by 10%. The athermal interfacial friction due to dislocation forest increases significantly as well. The interface velocity as a function of temperature and interface position is calculated. The decrease in the driving force and increase in the resistance lead to interface deceleration and to growth arrest. A transition from rate-dependent, thermally activated interface kinetics to athermal (rate-independent) kinetics at the macrolevel (in terms of the volume fraction of new phase) is demonstrated. At the same time, rather high internal shear stresses can promote nucleation in neighbouring regions of the stress-assisted martensitic variants with the same transformation shear (as in lath martensite packets) or with the opposite transformation shear (as in self-accommodated martensitic units). In § 4.2 the related problem of the appearance and growth of a martensitic unit near a free surface is treated. The free surface promotes plastic accommodation around the growing unit. After a significant decrease in the transformation work during a growth stage at distances from the free surface of 1.2–0.75 times the plate thickness the transformation work increases sharply. The athermal dislocation forest friction increases significantly in the same range of distance from the free surface and then decreases, giving a non-monotonic velocity. In § 4.3 the appearance and growth of a small interface step are studied. In contrast with the elastic growth regime, the thermodynamic conditions for lengthening and thickening are almost equivalent.

Direct tensor notations are used throughout this paper. Vectors are denoted in bold sans serif roman type and tensors are denoted in bold serif roman type; $\mathbf{A}\cdot\mathbf{B}$ $((\mathbf{A}\cdot\mathbf{B})_{ik} = A_{ij}B_{jk})$ and $\mathbf{A} : \mathbf{B} = A_{ij}B_{ji}$ are the contraction of tensors over one and two indices; $\mathbf{I}$ is the unit second-rank tensor; $\mathrm{dev}\,\mathbf{A}$ is the deviatoric part of $\mathbf{A}$; $|\mathbf{A}| := (\mathbf{A} : \mathbf{A}^{\mathrm{T}})^{1/2}$ is the modulus of tensor $\mathbf{A}$. A superscript T and -1 denote transpose and inverse operations; the subscripts s and a designate symmetrical and antisymmetrical tensor parts; $:=$ means equals per definition; a point above indicates the material time derivative.

§ 2. Problem formulation at finite strains

Consider a volume V of multiphase material with a boundary S and prescribed boundary data. Assume that some volume V_{n} with a fixed boundary Σ_{n} relative to the material's points undergoes the martensitic PT. The martensitic PT represents a special type of deformation of a crystal lattice from the parent phase (austenite) into a crystal lattice of product phase (martensite) without diffusion. This deformation is

called the transformation strain. In this paper we shall study the appearance and growth of a martensitic unit in an austenitic matrix (see figures 2 and 12 later). Here the martensitic PT will be considered as the thermomechanical process of growth of a transformation deformation gradient $\mathbf{F}_t$ in some transforming region V_n from unit tensor $\mathbf{I}$ to a final value $\bar{\mathbf{F}}_t$ determined by crystallography which is accompanied by a change in the mechanical and thermal material properties.

2.1. *Kinematics*

Let the motion of the deformed material in the process of martensitic PT be described by the function $\mathbf{r} = \mathbf{r}(\mathbf{r}_0, t)$, where $\mathbf{r}$ and $\mathbf{r}_0$ are the positions of points in the actual V and the reference V^0 (at $t = 0$) configurations; t is the current time. Thermal strains are neglected because they are small with respect to transformation strains. We present only the final set of equations (given in appendix A) in the form convenient for numerical algorithm (for derivation see Levitas (1998a) and Idesman *et al.* (1999)). We assume a multiplicative decomposition of the total deformation gradient $\mathbf{F} = \partial\mathbf{r}/\partial\mathbf{r}_0$ into the elastic part $\mathbf{F}_e$, transformational part $\mathbf{F}_t$ and plastic part $\mathbf{F}_p$ (see equation (A 1)), where $\mathbf{F}_e = \mathbf{V}_e \cdot \mathbf{R}_e$, with $\mathbf{V}_e$ the elastic left stretch (symmetric) tensor and $\mathbf{R}_e$ the elastic rotation tensor. We introduce the dimensionless order parameter $\xi\,(0 \leqslant \xi \leqslant 1)$ which is related to $\mathbf{F}_t$ and has the following properties: the PT starts at $\xi = 0$ and finishes at $\xi = 1$; when ξ varies between 0 and 1, the transformation deformation gradient grows from $\mathbf{I}$ to the final maximum value $\bar{\mathbf{F}}_t$. It is possible to define the order parameter ξ, for example, as $\xi := |\mathbf{F}_t - \mathbf{I}|/|\bar{\mathbf{F}}_t - \mathbf{I}|$. Using equation (A 1), one obtains for the velocity gradient $\mathbf{l}$

$$\mathbf{l} := \frac{\partial \mathbf{v}}{\partial \mathbf{r}} = \dot{\mathbf{F}} \cdot \mathbf{F}^{-1} = \dot{\mathbf{F}}_e \cdot \mathbf{F}_e^{-1} + \mathbf{l}_t + \mathbf{l}_p, \tag{1}$$

$$\mathbf{l}_t := \mathbf{F}_e \cdot \dot{\mathbf{F}}_t \cdot \mathbf{F}_t^{-1} \cdot \mathbf{F}_e^{-1}, \quad \mathbf{l}_p := \mathbf{F}_e \cdot \mathbf{F}_t \cdot \dot{\mathbf{F}}_p \cdot \mathbf{F}_p^{-1} \cdot \mathbf{F}_t^{-1} \cdot \mathbf{F}_e^{-1}, \tag{2}$$

where $\mathbf{v} = \dot{\mathbf{r}}$ is the velocity vector, and $\mathbf{l}_t$ and $\mathbf{l}_p$ are the transformation and the plastic parts respectively of the velocity gradients. A corresponding description of the deformation rate is given in equation (A 4).

To define uniquely the elastic and plastic parts of the total deformation gradient we assume that the modified plastic spin $\mathbf{W}_p$ is zero, that is

$$\mathbf{W}_p := (\mathbf{F}_e \cdot \mathbf{F}_t \cdot \dot{\mathbf{F}}_p \cdot \mathbf{F}_p^{-1} \cdot \mathbf{F}_t^{-1} \cdot \mathbf{F}_e^{-1})_a = \mathbf{0} \quad \text{and} \quad \mathbf{d}_p = \mathbf{l}_p. \tag{3}$$

This constitutive result can be derived for isotropic material by some extension and application of a method developed by Levitas (1998b) for the case with the PT. A similar assumption is accepted in many papers on large strains without the PT (for example Weber and Anand (1990) and Simo and Miehe (1992)). It allows us to determine the rate of plastic deformation gradient $\dot{\mathbf{F}}_p$ through the rate of plastic deformation $\mathbf{d}_p$.

We use the elastic strain tensor $\mathbf{B}_e$ defined by equation (A 2). We assume that the elastic strains are small, that is $\mathbf{V}_e = \mathbf{I} + \boldsymbol{\varepsilon}_e, \boldsymbol{\varepsilon}_e \ll \mathbf{I}$; then $\mathbf{V}_e^{-1} \approx \mathbf{I} - \boldsymbol{\varepsilon}_e$ and $\mathbf{B}_e \approx \boldsymbol{\varepsilon}_e$.

In the approach presented, the transformation deformation gradient $\mathbf{F}_t$ should be prescribed as input data. For the solution of the PT problem we vary it according to equation (A 3) when ξ grows from 0 to 1. To prescribe the final value of the transformation deformation gradient $\bar{\mathbf{F}}_t$ we use in this paper the simplest variant of crystallographic theory when the transformation strain is a deformation with an invariant (non-deformable and non-rotating) plane, corresponding to the habit

plane (Wayman 1964, Nishiyama 1978) of the transformation unit (e.g. lath or plate).

For a material point without a PT we must prescribe in the above equations that $\mathbf{F}_t = \mathbf{I}$ before PT or $\mathbf{F}_t = \bar{\mathbf{F}}_t = \text{constant}$ after PT.

2.2. *Constitutive equations*

We use a thermodynamically consistent system of constitutive equations at large strains for isotropic elastoplastic materials with PT and isotropic hardening, presented in Appendix A. Detailed derivation of the equations in Appendix A can be found in the papers by Levitas (1998a) and Idesman *et al.* (1999). Here q is the accumulated plastic strain, $\sigma_i = (\frac{3}{2}\mathbf{s} : \mathbf{s})^{1/2}$ is the stress intensity, $\mathbf{s} = \operatorname{dev}\mathbf{T}$ is the deviatoric part of the Cauchy stress tensor $\mathbf{T}$, $\sigma_y(q, \xi)$ is the yield stress, as determined experimentally, $\mathbf{E}$ is the elastic modulus tensor, K and G are the compression and shear elastic moduli respectively, and $I_1(\mathbf{B}_e) = \mathbf{I} : \mathbf{B}_e$ is the first invariant of $\mathbf{B}_e$.

2.3. *Mesoscopic transformation criterion, kinetic equation and extremum principle for phase transformation*

In this section we shall combine the continuum thermodynamic approach for determination of the driving force developed by Levitas (1998a, 2000) with physically based and experimentally verified equations for athermal and thermal parts of the interface frictional force (Olson and Cohen 1986, Ghosh and Olson 1994). Assume that material in some volume V_n undergoes the PT. The volume can belong to the new nucleus or to a region traversed by its moving interface; the procedure for the derivation of the thermodynamic transformation condition is the same (Levitas 1998a). Assume that the volume V_n is obtained by the interface Σ propagation with a normal velocity v_n in time Δt, that is it is bounded by surfaces Σ_t and $\Sigma_{t+\Delta t}$ at times t and $t + \Delta t$ respectively, as well as by two lateral infinitesimal surfaces with the heights $v_n \Delta t$. In figure 2, each of regions II, III, IV and V corresponds to such a volume V_n owing to subsequent growth of initial region I. As the transformation volume change in our problem is taken as 2.6% appropriate for an Fe–Ni alloy, the elastic volume change is negligible and the material is plastically incompressible, we assume that the mass density $\rho(\xi) \approx \rho = \text{constant}$. Thus we need not distinguish the interface velocity with respect to austenite and martensite.

Let us fix the surface $\Sigma_{t+\Delta t}$ and consider the PT process in a fixed volume $\mathrm{d}V_n = v_n \Delta t \, \mathrm{d}\Sigma_t$ (figure 2). It appears that, owing to the infinitesimal height $v_n \Delta t$, the results are independent of the details of the process inhomogeneity along the height. At the same time, because of the history-dependent character of the constitutive equations for inelastic materials, we must in any case consider the transformation process at the transforming points. Therefore we consider homogeneous growth of a transformation deformation gradient from unit tensor $\mathbf{I}$ to a final value in a finite transforming region V_n. This includes both the appearance of a new martensitic region and its growth modelled as a locally homogeneous deformation process in the incremental region II, then region III and so on (figure 2).

The key points of our approach are as follows (Levitas 2000). Using the second law of thermodynamics, the dissipation rate $\mathcal{D}$ due to PT only is separated from other dissipative contributions (e.g. due to plastic deformation) and expressed in the following form:

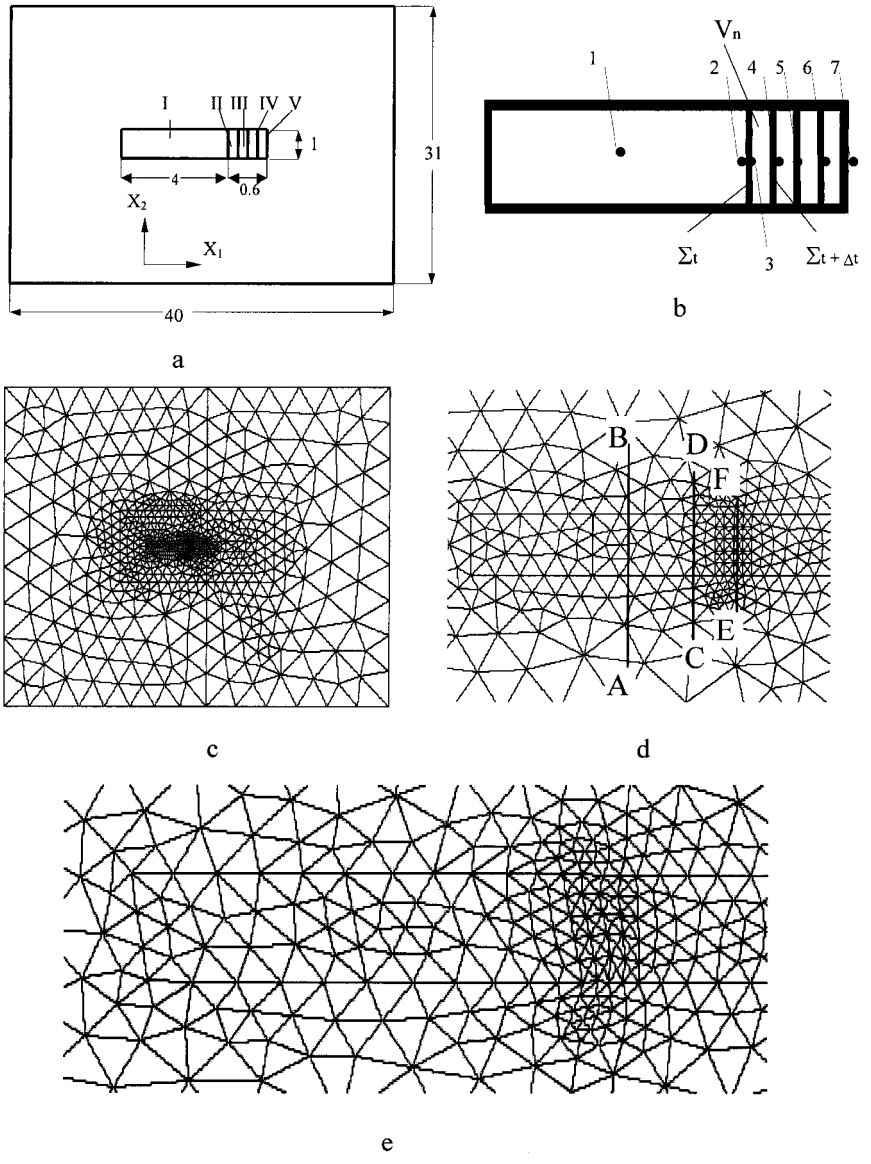

Figure 2. Cross-section of a sample with (*a*) subsequently transforming regions I–V, (*b*) transforming regions and (*c*)–(*e*) finite element meshes before ((*c*) for a whole sample; (*d*) near transforming regions) and after ((*e*) near transformations regions) transformation.

$$\mathcal{D} := X_{\mathrm{v}}\dot{\chi}, \tag{4}$$

$$X_{\mathrm{v}} := \bar{X} m_{\mathrm{n}} := \int_{V_{\mathrm{n}}} X \,\mathrm{d}V_{\mathrm{n}} - \Delta\Gamma, \quad \dot{\chi} := \frac{1}{t_{\mathrm{s}}}, \tag{5}$$

$$X := \int_0^1 \mathbf{T} : \mathbf{d}\,\frac{\mathrm{d}t}{\mathrm{d}\xi}\,\mathrm{d}\xi - \rho\,\Delta\psi - \int_{\theta_1}^{\theta_2} \rho s \,\mathrm{d}\theta - \int_0^1 \mathbf{T} : \mathbf{d}_{\mathrm{p}}\,\frac{\mathrm{d}t}{\mathrm{d}\xi}\,\mathrm{d}\xi, \tag{6}$$

with explicit expressions for the generalized (driving) force X_v and rate $\dot{\chi}$. The force X_v is the total dissipation increment due to PT only (excluding plastic and other types of dissipation if they are included in the description) during the complete PT in the transforming region; the rate $\dot{\chi}$ is the inverse PT duration t_s. Here m_n is the mass of the transforming region, $\bar{X}$ is the driving force per unit mass which will be used later, $\Delta\psi$ is the increment of the Helmholtz free energy, s is the specific entropy, θ is the temperature, $\Delta\Gamma$ is the increment of the total surface energy of transforming volume and the indices 1 and 2 denote the values before and after PT. As is usual in kinetic theory, a kinetic relation (response function) between force and rate, $X_v = K_v(\dot{\chi}, \ldots)$ (or between rate and force which can be expressed in the form $t_s = F(X_v, \ldots)$; see equation (A 15)), must be specified.

For interface propagation assuming that each infinitesimal volume $dV_n = v_n \Delta t \, d\Sigma$ transforms independently of the other, we obtain that the driving force is defined locally at each point of the interface and the rate of dissipation per unit $d\Sigma$ with allowance for $\Delta t = t_s$ has the form

$$\mathcal{D}_\Sigma := \frac{\mathcal{D}}{d\Sigma} = \frac{\bar{X}\rho v_n \, d\Sigma \, t_s}{d\Sigma t_s} = \rho \bar{X} v_n. \tag{7}$$

Consequently, $\bar{X}$ and v_n are the driving force and rate respectively, and an interface mobility equation $\bar{X} = K(v_n, \ldots)$ must be prescribed. The theoretical form of the martensitic interface mobility has to be derived through an extension of thermally activated deformation theory, and experimentally verified in single-interface experiments in thermoelastic systems (Grujicic, Olson and Owen 1985). Mobility parameters for non-thermoelastic ferrous alloys have been determined by interpreting isothermal nucleation kinetics in terms of interface-controlled barrierless heterogeneous nucleation (Olson and Cohen 1986). The required driving force K consists of two parts (Olson and Cohen 1986, Ghosh and Olson 1994):

(i) the athermal component K_0 due to long-range fields (barriers), which is rate independent and represents the dissipative threshold, that is at $\bar{X} < K_0$ the PT transition does not occur and $v_n = 0$;
(ii) the thermal component K_{th} due to short-range fields (barriers) which can be overcome by thermal fluctuations.

The athermal part K_0 consists of a solute atom contribution K_μ and a dislocation forest hardening contribution K_d. For the athermal dislocation forest hardening the following relation for Fe–22.31 wt% Ni–2.888 wt% Mn alloy was measured from martensite kinetic measurements in pre-strained samples by Ghosh and Olson (1994):

$$K_d = Aq^{0.5} = B[\sigma_y^a(q) - \sigma_y^a(0)], \quad A = 60.33\,\text{MPa}, \quad B = 0.0928, \tag{8}$$

where the corresponding expression for the experimentally determined flow curve for slip deformation of austenite,

$$\sigma_y^a(q) = \sigma_y^a(0) + \frac{A}{B} q^{0.5},$$

is used. A similar relation $K_0 = L\sigma_y^a(q)$ was derived by Levitas (1997, 1998a) based on high-pressure experiments. We shall use the first of equations (8) for our estimation of the effect of accommodational plastic deformation on athermal friction for interface propagation conditions equation (A 11) and (A 13) with substitution of q

with $\bar{q} := (1/V_n)\int_{V_n} q_{(\xi=0)}\,\mathrm{d}V_n$ calculated before the start of PT and averaged over the transforming zone.

Let us consider an infinitesimal m_n and Δt and neglect for simplicity the change in surface energy; then, for each point of the interface, $\bar{X} = X$. Using the Hadamard compatibility and traction continuity conditions, the first term in equation (6) (the stress work) can be simplified (Levitas 1998a). Then the first two terms in equation (6) represent the standard Eshelby (1970) driving force at the moving interface: $X_e := \mathbf{T} : [\mathbf{F}_{21}] - \rho\Delta\psi$, where $[\mathbf{F}_{21}] := \mathbf{F}_{21} - \mathbf{I}$ is the jump in deformation gradient when the actual state before the PT is considered as the reference configuration. Note that, in most known papers devoted to interface propagation conditions in plastic materials, the kinetic equation for interface motion has the form $X_e = K(v_n, \ldots)$ (see the papers by Kondaurov and Nikitin (1986), Fischer *et al.* (1994, 2000), Simonsson (1995), Fischer and Reisner (1997), Cherkaoui *et al.* (1998), Cherkaoui and Berveiller (2000) (in most cases with $K =$ constant)). In papers by Roitburd and Temkin (1986), Kaganova and Roitburd (1987, 1989), interface equilibrium and propagation in elastoplastic materials for a particular geometry (sphere or ellipsoid) are considered in an alternative but simplified way; see the analysis in the paper by Levitas (1998a). The necessity to extract plastic work from the Eshelby driving force was demonstrated in the papers by Levitas (1998a, and references herein); allowance for the temperature variation in the same form as in equation (6) was made in the same papers.

The Eshelby driving force can be calculated if we know the state from both sides of the fixed interface and this is sufficient for the description of PT in elastic materials. In order to calculate integrals over the transformation process in equation (6) for plastic materials we have to produce the transformation process, that is again we have to consider PT in the infinitesimal volume covered by the moving interface. For numerical calculation we consider a small but finite volume transforming at the interface.

To simplify the final expression for $\bar{X}$ we assume that both phases have the same elastic properties; the temperature does not change during the transformation process and is uniform. Then we obtain equation (A 12) for the driving force $\bar{X}$ (for details see Levitas (1998a) and Idesman *et al.* (1999)), where φ is the transformation work per unit mass of transformed region and $\Delta\psi^{\theta}$ is the difference between the thermal (chemical) parts of the specific Helmholtz free energy which is an experimentally determined function of temperature. Using the dependence of K_{th} on the interface rate v_n and temperature formulated in the papers by Ghosh and Olson (1994), the interface propagation equation (A 13) can be derived. Here v_{n0} is the characteristic velocity which is of the order of the shear-wave velocity, Q_0 is the activation energy, W_0 is the height of the driving force barrier corresponding to the rate-controlling obstacles (at $\bar{X} - K_0 \geqslant W_0$, equation (A 13) is not valid, because interface motion does not require thermal fluctuations), k is the Boltzmann constant and p and b are constants. All material parameters estimated for Fe–22.31 wt% Ni–2.888 wt% Mn alloy are presented in table 1.

The parameters $p = 0.5$ and $b = 1.5$ in equation (A 13) are predicted theoretically (Kocks *et al.* 1975, Grujicic *et al.* 1985) for the interaction of interfacial dislocations with the strain field of solute atoms. These parameters allowed the best fit of experimental data for normalized activation energy versus normalized driving force for a number of steels (Ghosh and Olson 1994). The characteristic velocity v_{n0} is of the order of the shear-wave velocity and is found to be $3000\,\mathrm{m\,s^{-1}}$ (Grujicic *et al.* 1985).

Table 1. Material parameters for Fe–22.31 wt% Ni–2.888 wt% Mn alloy.

A (MPa)	B	W_0 (MPa)	K_μ (MPa)	Q_0 (J)	v_{n0} ($m\,s^{-1}$)	p	b
60.33	0.0928	59	2.35	2.1×10^{-19}	3000	0.5	1.5

The parameters W_0, K_μ and Q_0 are determined from the best fit of the experimentally determined temperature dependence of activation energy for annealed ferrous alloys. The parameters A and B are determined by the best fit of the same plot for austenite pre-deformed to various magnitude of plastic strain (Ghosh and Olson 1994). It is found that resistance to interface motion due to dislocation forest hardening is one order of magnitude higher than K_μ; so, the possible error in $K_\mu$is not significant.

For the thermal part of the free-energy change we use (Haezebrouck 1987)

$$\Delta\psi^\theta = 0.708\theta - 308\,\text{MPa}.$$

The interface propagation criterion (A 11) and kinetic equation (A 13) combine the advantage of the strict continuum thermodynamic derivation of the expression for the driving force $\bar{X}$ with physically based equations for the athermal and thermal parts of the frictional force.

It is necessary to note that the PT equations (A 11)–(A 13) include the history of stress $\mathbf{T}$ variation in the transforming region during the PT and plastic strain q variation in the transforming region before the PT. We have to solve the elastoplastic problem in order to calculate the transformation work φ and $\bar{q}$ in equation (A 12).

We shall consider as well the PT in some region without the assumption that it is related to uniform interface motion. This will be done when we introduce a small step which then moves along the interface making the PT. In this case we shall use the transformation criterion (A 14) and kinetic equation (A 15). The concrete function F given in the paper by Levitas (2000) will not be used here; however, the important point that it depends on X_v rather than on $\bar{X}$ has to be stressed.

In a general case the position, shape and volume of a new transforming region are unknown. For a PT in elastic materials the principle of the minimum Gibbs free energy can be used. For inelastic materials the principle of maximum transformation rate $\dot{\chi}$ or minimum transformation time (A 16) is derived (Levitas 2000) using the postulate of realizability (Levitas 1997, 1998a). Here the superscript asterisk means that the parameters $\bar{X}^*$ and m_n^* are determined at the PT in some possible (trial) PT region V_n^* and the principle (A 16) prescribes the actual transforming region V_n among all possible V_n^*. The physical interpretation of the principle (A 16) is very simple; as soon as the PT can occur (i.e. when the PT criterion (A 14) is satisfied), it will occur during the time determined by the kinetic equation (A 15) for each chosen transforming volume V_n^*. Then we shall observe the PT which appears in the shortest time, that is we arrive at the *principle of minimum transformation time*.

§ 3. Numerical method

A general scheme for the application of PT criteria (A 12) and (A 14) and kinetic equations (A 14) and (A 15) is as follows. All the material properties and constitutive equations must be given for each intermediate state of PT, that is for $\xi \in [0, 1]$. Then assume that, at some prescribed initial and boundary conditions, PT occurs in some

region V_n either covered by moving interface during time Δt or in a new nucleus. We introduce the transformation strain and change the material properties from initial to final values incrementally in a PT region. After solving the elastoplastic boundary-value problem for each step we determine the variation in all the fields, calculate the driving force $\bar{X}$ (A 12) and resistance K^0 (equation (A 11)) and at $\bar{X} - K^0 \geqslant 0$ determine the interface velocities (equation (A 13)) or the PT time t_s from equation (A 15).

We do not present here the numerical algorithm developed which has been described in detail in the paper by Levitas *et al.* (1998) for small strains and in the papers by Idesman *et al.* (1999) for finite strains for PT and twinning. We note only its main characteristic features. For spatial discretization the FEM is used (quadratic triangular finite elements are used for all the model problems considered below).

In the numerical approach considered in this paper, the PT region is assumed to be given in advance (the ways to determine the PT region have been proposed and discussed in the paper by Levitas *et al.* (1998)). Then, in order to calculate the variation in the stress–strain state during the PT we have to solve an elastoplastic problem incrementally with the prescribed transformation deformation gradient $\mathbf{F}_t$ in the region where the PT is assumed to occur. Such a formulation for the PT is kinematically similar to the problem of thermoplasticity with anisotropic thermal expansion, that is the order parameter ξ can be treated like the temperature, and the transformation deformation gradient like the thermal deformation gradient. At small strains, such a problem for the PT is solved by well-known numerical algorithms for thermoelastoplasticity in all the studies on PT which were available to the present authors (for example Ganghoffer *et al.* (1991), Marketz and Fischer (1994a, 1994b), Fischer and Reisner (1997) and Levitas *et al.* (1998)). At finite strains an extension of the algorithms based on the multiplicative decomposition of the deformation gradient was proposed in a paper by Idesman *et al.* (1999) for the case with PT and twinning. The solution of the nonlinear elastoplastic problem at large strains is based on a Newton–Raphson iterative scheme. The use of the current configuration and the true Cauchy stresses together with assumptions of small elastic strains and the condition of zero modified plastic spin allows us to apply the radial return algorithm for the stress calculation and to derive quite a simple formula for the consistent elastoplastic moduli for the calculation of the consistent tangent stiffness matrix in the Newton–Raphson iterative scheme. Some modifications of the iterative algorithm related to the numerical integration of constitutive equations together with the radial return algorithm are suggested in order to improve the accuracy of solutions for large increments in external load (such modifications can be used for any elastoplastic problem without a PT as well).

§ 4. Numerical study of appearance and growth of a martensitic particle

To study in detail the stress–strain fields, the thermodynamic and kinetic conditions of martensitic unit growth in elastoplastic materials using the interface propagation criterion (A 11) and the kinetic equation (A 13) we solve a number of model boundary-value problems. The following simplifying assumptions are presumed:

(i) The elastic properties of austenite and martensite in steel are taken as identical (which is a good approximation for steel); Young's modulus $E = 2 \times 10^5$ MPa, Poisson's ratio $\nu = 0.3$.

(ii) Both phases are perfectly plastic; the yield stress $\sigma_y^a = 2.5 \times 10^2$ MPa for

the austenitic matrix and $\sigma_y^m = 8 \times 10^2$ MPa for the martensite (Marketz and Fischer 1994b). It is not a problem to include a hardening rule. However, the plastic properties of martensite and, in particular, of a single martensitic plate are not well defined. First, martensite inherits the plastic strain accumulated in austenite, and it is not clear how it affects its stress–strain curve. Second, a large plastic deformation occurs during the transformation event, and again it is unknown which hardening rule can be used. Because of this uncertainty, and because, at such a large strain, hardening is saturated (i.e. the behaviour tends to perfectly plastic), it seems to us inappropriate to consider a more complex model than the perfectly plastic material. An important point for modelling is that the yield stress of martensite is much larger than the yield stress of austenite.

(iii) The yield stress in the transforming region changes instantaneously to the value of the product phase at the beginning of the PT ($\xi = 0$).

(iv) The case of the plane-strain state is considered. This is a good approximation, because the transformation strain (which is the reason for the stresses and plastic strain) is a plane strain.

(v) The inverse problem is solved, that is the position and size of the transforming region are specified *a priori*, and then the condition for PT is determined.

(vi) The transformation deformation gradient in each subsequently transforming region increases homogeneously from the unit tensor to the final value $\bar{\mathbf{F}}_t$ according to equation (A 3); $\mathbf{F}_t$ has the following components (Nishiyama 1978, Marketz and Fischer 1994b) in the Cartesian coordinate system with the normal $\mathbf{n}$ directed along the axes X_2 (figure 2):

$$(\bar{F}_t)_{11} = 1, \quad (\bar{F}_t)_{12} = 0.2, \quad (\bar{F}_t)_{21} = 0, \quad (\bar{F}_t)_{22} = 1.026, \quad (\bar{F}_t)_{33} = 1,$$
$$(\bar{F}_t)_{31} = (\bar{F}_t)_{32} = (\bar{F}_t)_{13} = (\bar{F}_t)_{23} = 0. \tag{9}$$

(vii) The boundary of the sample is free from stresses, which corresponds to experiments for temperature-induced PT.

(viii) Displacements at the austenite–martensite interface are continuous (coherent interface).

(ix) The temperature is homogeneous and does not change during the PT.

For our calculations the transformation deformation gradient $\bar{\mathbf{F}}_t$ and the order parameter ξ are subdivided into 60 increments. Solving the elastoplastic problem with incrementally enlarged transformation deformation gradient in a given transforming region we calculate stress–strain fields as well as the value of the transformation work φ and averaged accumulated plastic strain $q_{(\xi=0)}$ before PT. Then, at a given temperature, $\Delta\psi^\theta$ as well as K_μ are known; hence this gives full information for evaluating the possibility of PT (equation (A 11)) and interface velocity (equation (A 13)).

4.1. *Appearance and growth of a martensitic particle inside the austenitic matrix*

The cross-section of a sample is given in figure 2; the thickness of a transformed unit is of the order of 1 μm. We carried out calculations for the simultaneous PT in region I (appearance of the martensitic unit) and then subsequent PT in regions II–V, that is first in region II, then in region III and so on.

Consideration of the homogeneous increase in the transformation deformation gradient from the unit tensor to the final value in the region I is an approximate way to find an initial condition for the study of the growth process. Of course, the results depend on the aspect ratio of unit I (Idesman *et al.* 1999, 2000) and on the actual transformation process. However, modelling of an actual heterogeneous nucleation process requires consideration on a significantly smaller scale $h \approx 10^{-3}$–10^{-1} μm and the use of a discrete dislocation model. This would be necessary to simulate the real stress concentration at a nucleation size and the transition from elastic growth to plastic by nucleation and multiplication of dislocations. This complex problem is beyond the scope of this paper. To study the mesoscopic features of supercritical martensite growth in a reasonable computation time we made the above choices for the problem formulation consistent with previous treatments of nucleation details (Olson and Cohen 1986, Haezebrouck 1987). Note that a simplified way to determine the initial size of a thermodynamically admissible nucleus based on the same finite-element solution as here and the extremum principle (A 16) is realized in the paper by Idesman *et al.* (2000). Here we shall calculate the transformation work for the appearance of supercritical site unit I only to compare it with the transformation work for interface propagation.

We used a refined finite-element mesh in and near the transforming zone. Each transforming region during unit growth (II, III, IV and V) contains 20 finite elements. The space increment for interface motion (width of regions II, III and so on) is chosen to be 0.15 of the unit width and the initial width of plastic zone after appearance of unit I (figures 2 (*c*) and 3 (*a*)).

It is convenient to introduce the process parameter ζ as follows: $\zeta = \sum_{i=1}^{k} \xi_i$, where k designates the number of the transforming region in figure 2 and ξ_i is the order parameter ξ in region i. For example, when $k = 1$, the PT occurs in the large unit I and $\zeta = \xi_1$. After finishing the PT in the region and starting the transformation in region II, we have $k = 2$, $\xi_1 = 1$ and $\zeta = 1 + \xi_2$. When the PT is completed in region II and starts in region III, then $k = 3$, $\xi_1 = \xi_2 = 1$ and $\zeta = 2 + \xi_2$ and so on.

The deformed mesh in the transformed region (figure 2 (*e*)) together with isobands of accumulated plastic strain (figures 3 and 4) present overall very complex and heterogeneous strains and consequently stress fields in austenite and martensite and their non-monotonic time variation (with time represented by the process parameter ζ). As the transformation shear is taken as negative, positive values of shear stress and plastic shear strain correspond to the direction opposite to transformation shear. We shall use the terms 'forward' shear relative to the direction of the transformation shear in regions I–V if it has a negative sign and 'reverse' shear in the opposite case. Eventual new martensitic variants near regions I–V with forward (or reverse) transformation shear will be called forward (or reverse) variants.

Shear stresses in martensite are distributed very heterogeneously in the transforming zone on the appearance of the martensitic unit and especially during its growth (figure 5). Stresses in the most part of the unit are in the interval 156–281 MPa. The assumption of a homogeneous field inside the ellipsoidal inclusion and the application of the Eshelby solution are rather rough approximations (that was also indicated for the case of small elastoplastic strains by Marketz and Fischer (1994a,b)).

The analysis of the shear stress distribution in austenite (figure 6) is very important from the viewpoint of estimating autocatalytic nucleation sites. As will be concluded below, plastic growth can be arrested and the appearance of new nuclei is

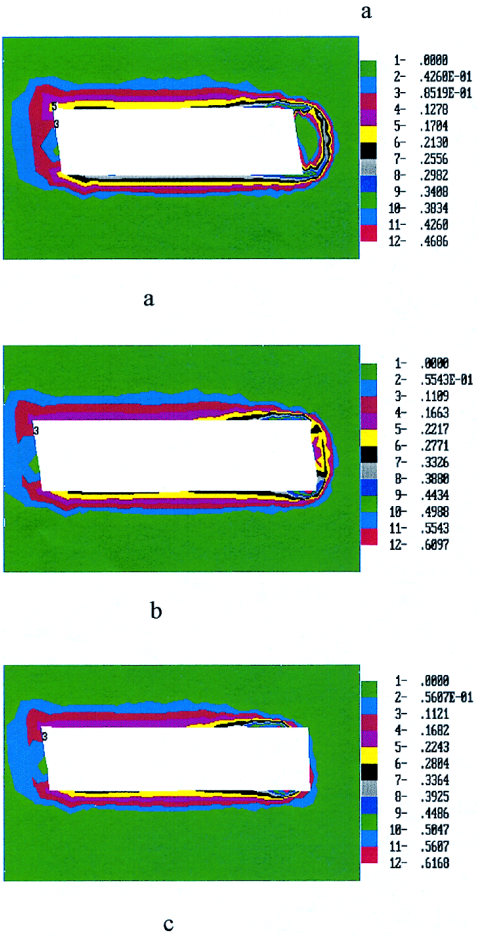

Figure 3. Isobands of the accumulated plastic strains near transformation regions after transformation in (*a*) region I, (*b*), regions I–III and (*c*) regions I–V.

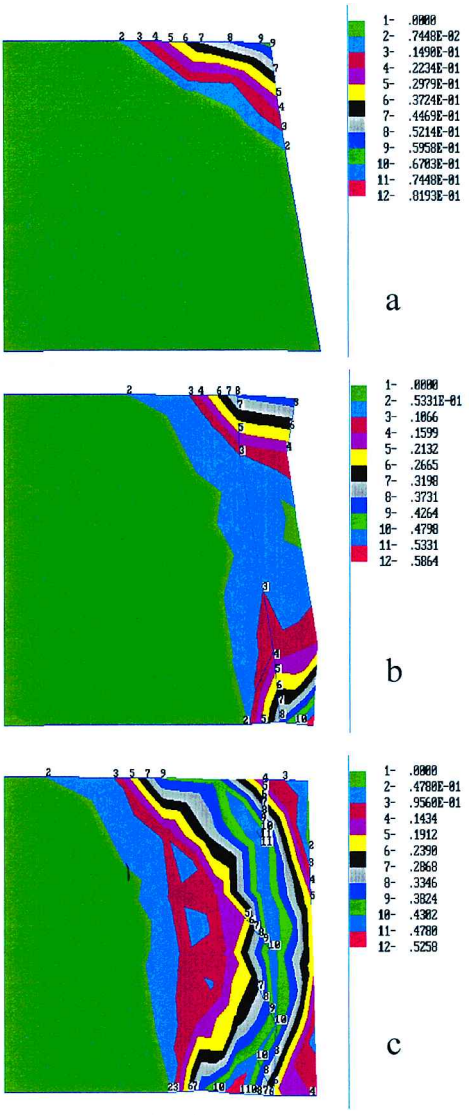

Figure 4. Isobands of the accumulated plastic strains in the right part of the martensitic unit after transformation in (*a*) region I, (*b*) regions I–III and (*c*) regions I–V.

necessary to continue the PT. After the appearance of the martensitic unit there is a wide band (red, blue and green colours in figure 6 (*a*)) in which the shear stress varies in the range 70–184 MPa and can cause the nucleation of stress-induced reverse martensitic variants which are often observed in self-accommodated martensite aggregates. Near the short sides of the martensitic region and near upper right and lower left corners (brown and purple colours) the shear stress varies in the range from −82 to −182 MPa and can produce stress-induced forward martensitic variants which are observed in a packet of lath martensite. During the growth of the

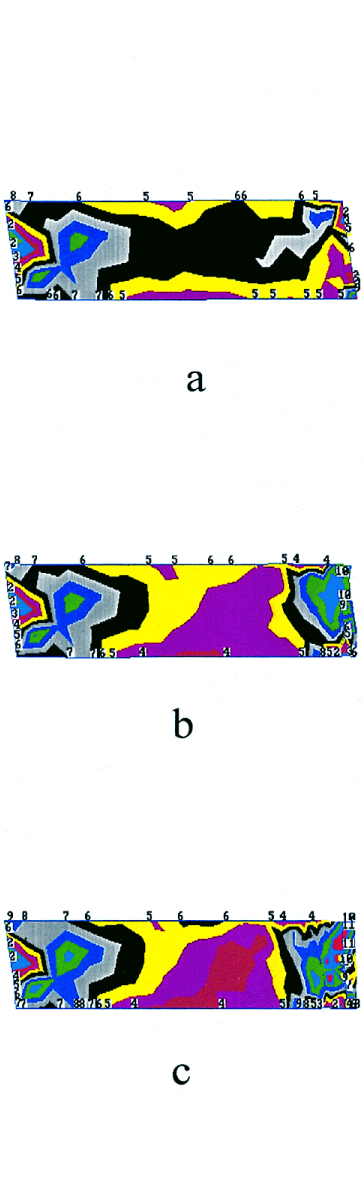

Figure 5. Isobands of shear stress in martensite after transformation in (*a*) region I, (*b*), regions I–III and (*c*) regions I–V.

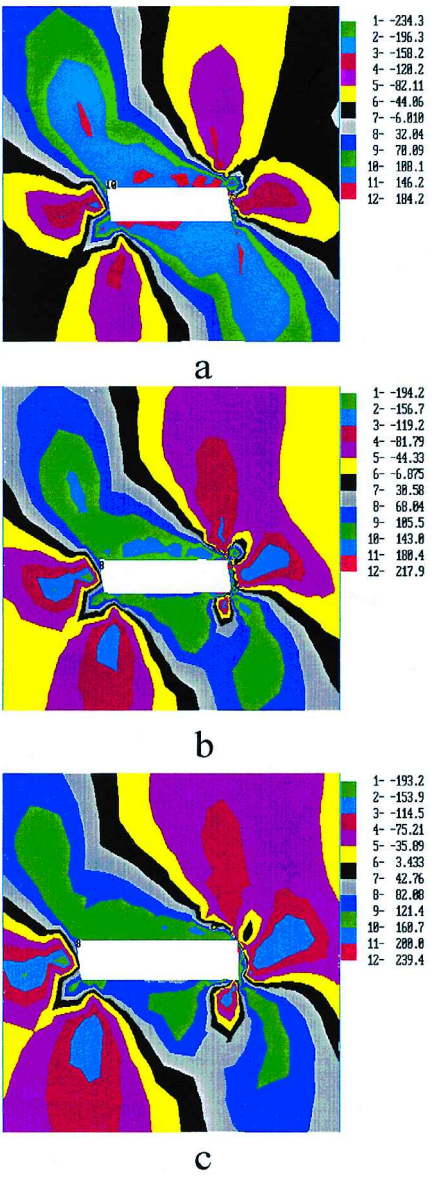

Figure 6. Isobands of shear stress in austenite near transformation regions after transformation in (*a*) region I, (*b*) regions I–III and (*c*) regions I–V.

particle (figures 6 (*b*) and (*c*)) the region of eventual appearance of forward martensite grows slightly and a new region (below the right lower particle corner) appears.

The transformation work decreases significantly from the value of -50.3 MPa for the appearance of a large region I to -100.8 MPa for region V with saturation which is expected for the steady stage of martensitic unit growth (figure 7). Such a decrease is caused by interaction between, firstly, the transformation strain in the currently transforming region, secondly, the transformation strain in the previously

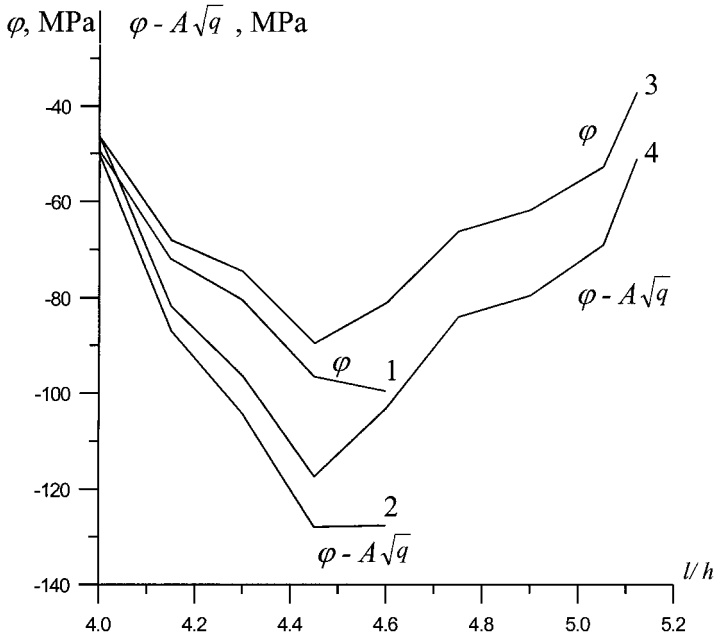

Figure 7. Transformation work φ and the difference $\varphi - A\bar{q}^{0.5}$ as functions of the aspect ratio l/h. Curves 1 and 2 correspond to the problem shown in figure 2, and curves 3 and 4 correspond to the problem shown in figure 12.

formed region and thirdly, the plastic strain field due to the previous transformation process and due to currently growing transformation strain as well as to the three-fold higher yield stress of martensite. At the same time the forest hardening term $A\bar{q}^{0.5}$ is equal to 13.94, 22.81, 30.22 and 26.84 MPa for the PTs in regions II, III, IV and V respectively, which is equivalent to a reduction in the driving force by the same values. In our case the term $A\bar{q}^{0.5}$ due to dislocation forest hardening is one order of magnitude higher than the resistance K_μ due to solution hardening.

The relationships between the logarithm of the interface velocity and temperature for the parameters φ and $A\bar{q}^{0.5}$ corresponding to their values in each region I–V are presented in figure 8 (the curves for regions IV and V coincide). The vertical lines I*–V* correspond to fulfilment of the thermodynamic interface propagation criterion. However, at fulfilment of this criterion the interface velocity is too small for each transforming region. If we assume that the detectable interface velocity is of the order of $10^{-2}\,\mu\mathrm{m\,s^{-1}}$, then we obtain a kinetic criterion of interface propagation. As follows from figure 8, the difference between the temperatures which correspond to the thermodynamic and kinetic propagation criteria varies from 5 K for region I to 15 K for region IV. If the martensitic region nucleates at $\theta = 270$ K, then at position I the interface propagates with maximum velocity; the velocity sharply decreases to $v_n = 10^6$ for region II and to $v_n = 10^{-2}$ for region III. Then the interface is arrested, because the PT criterion for region IV is not fulfilled.

Consequently, termination of the growth of a martensitic unit inside the grain, which is typical for formation of the lath martensite, is obtained in our model as a result of interaction of stress and plastic strain fields with a moving interface. It is necessary to reduce the temperature to 235 K to obtain a steady-state interface

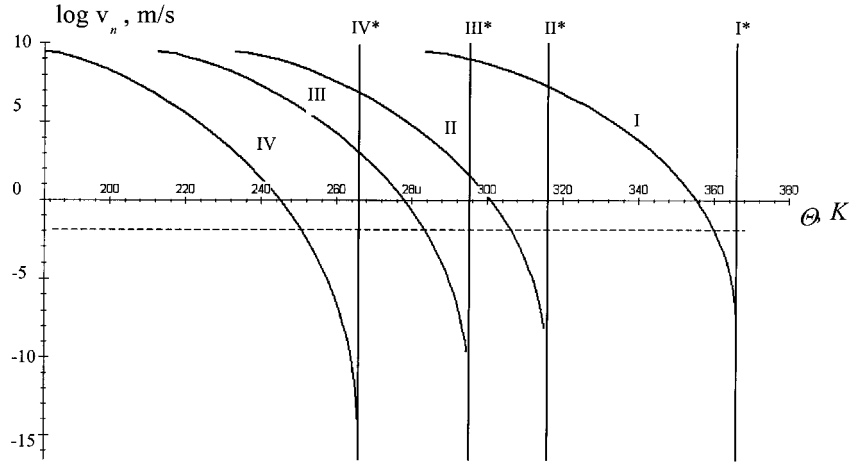

Figure 8. Interface velocity versus temperature for various interface positions after PT in regions I–V. Curves I, II, III and IV correspond to the kinetic equation (A 13) after sequential PT in regions I, II, III and IV respectively.

velocity of the order of $v_n = 10^{-2}\,\mu\mathrm{m\,s^{-1}}$. However, at such a cooling, new nuclei may appear near the arrested interface, forming a lath martensite packet.

If one assumes time-independent nucleation, then the result obtained illustrates also the transition from time-dependent thermally activated kinetics at the interface level to time-independent (athermal) kinetics at the macrolevel. This means that the volume fraction of martensite varies at cooling only and is independent of the cooling rate. This transition is related to the fact that, independent of interface velocity, growth is arrested after some interface progress owing to violation of the kinetic interface propagation criterion.

In figure 9 the variations in the shear stress $\bar{\tau} := (1/V_n)\int_{V_n} \tau\,\mathrm{d}V_n$, averaged over each region I–V during the sequential PT in regions I–V, are presented. In figure 10 the local plastic shear strain $\gamma := (F_p)_{12}$ variation is shown during the sequential PT in regions I–V at the points designated in figure 2(*b*) by the same numbers. All horizontal lines in figure 10 correspond to elastic behaviour of preliminary plastically deformed points and regions.

To obtain a simplified solution necessary for microscopic-to-macroscopic transition, in the paper by Cherkaoui *et al.* (1998) an assumption is used that the jump of plastic strain tensor across the interface is zero. As can be seen from a comparison of figures 3 and 4 as well as from figure 10, the jump in plastic strains is very significant. For example, at the appearance of the martensitic unit the accumulated plastic strain in it (figure 3) is zero (excluding the upper right and lower left corners, where the maximal value of q reaches 0.08), while in the matrix it reaches 0.46. When the PT in region III is finished, that is $\zeta = 3$, the plastic shear $\gamma = -0.58$ at point 6 (at the interface from the austenite side) and $\gamma = 0.32$ at the point 5 (figure 10), that is the jump in plastic shear reaches 0.90! Despite the fact that point 5 is not at the interface, the same value of γ occurs at the interface; this follows from the distribution of γ, which is not presented here, and from the distribution of the accumulated plastic strain (figure 4(*b*)), which is homogeneous along the line between points 5 and 6. It is necessary to mention that the use of the assumption that the jump in plastic strain is

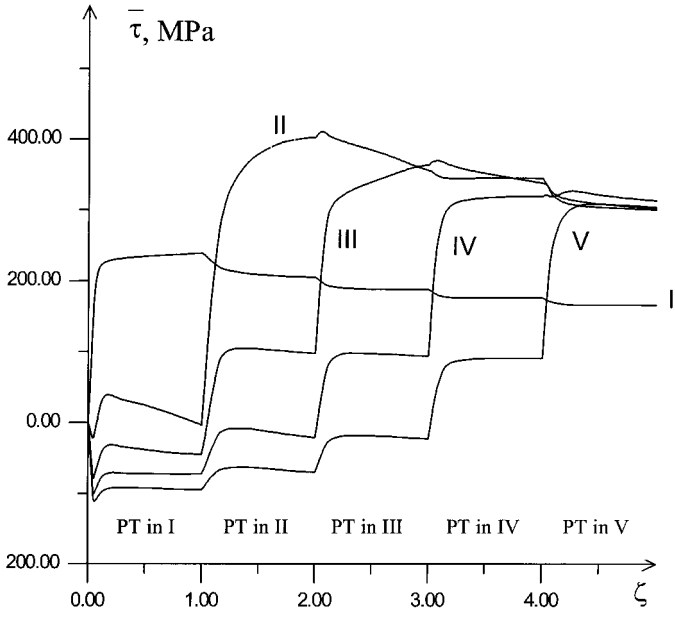

Figure 9. Variation in shear stress $\bar{\tau}$ averaged over each of regions I, II, III, IV and V (designated near the curves) during sequential phase transformation in regions I, II, III, IV and V.

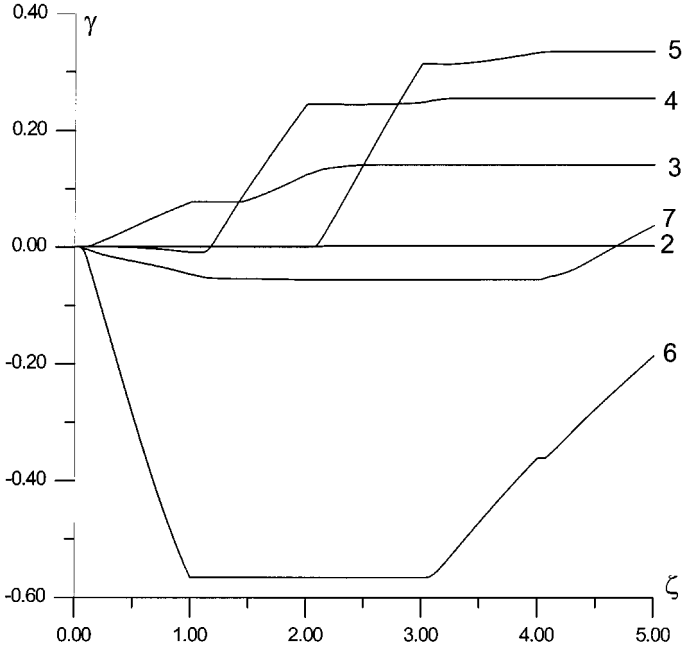

Figure 10. Variation of plastic shear strain at seven points (shown in figure 2 (*b*)) during the sequential phase transformation in regions I–V.

zero (which is not correct) in the interface propagation criterion $X_e = K$ used in the paper by Cherkaoui *et al.* (1998) (which is also not correct because plastic dissipation is not excluded) reduces the driving force X_e to $\bar{X}$ which was derived in the paper by Levitas (1998a) and used here, that is two errors compensate each other and the final thermodynamic PT condition used in the paper by Cherkaoui *et al.* (1998) is correct.

During the transformation in the large unit I, the local plastic shear strains at points 1 and 2 (figure 10) as well as the averaged plastic shear strain are very small; the accumulated plastic strain averaged over region I reaches 0.028 and does not change during the PT in regions II–V. The averaged shear stresses which resist the transformation strain grow very intensively (linearly) in the elastic regime and they are almost constant in the plastic regime (figure 9). The local shear stress at points 1–7 behaves similarly.

It was expected that the local shear stress and plastic strain in the points contacting the currently transforming region as well as the shear stress and plastic strain averaged over the region contacting the currently transforming region have the same sign as the transformation strain. It appears, however, that owing to very strong stress heterogeneity this is not the case. During the PT in region I the local shear stress and plastic strain at point 3 as well as the shear stress and plastic strain averaged over region II are positive. The same situation arises for all the other transforming regions.

Because of the large field gradients near the transforming region, the local shear stress and plastic strain in the points which are not in contact with the currently transforming region as well as the shear stress averaged over these regions have the same sign as the transformation strain. For example, during the transformation in particle I the shear stress at points 4–7 and the shear stress averaged over regions III, IV and V are negative. The shear plastic strain is almost zero at point 4, zero at point 5 and negative at points 6 and 7. In region III, owing to large gradients, the situation is very unexpected, because the shear stress and plastic strain averaged over this region have opposite signs. The averaged shear plastic stresses in regions IV and V have the same negative sign as the averaged shear stress.

In the transformation in region II, both the local shear stress at point 3 and the shear stress averaged over region II (which resist the transformation) grow significantly owing to the jump-like change in the yield stress. This is the reason for the decrease in transformation work in comparison with that for region I. At some later stage of transformation, the stress becomes high enough to cause plastic straining in martensite in addition to the plastic strain inherited by martensite from austenite.

With the transformation in region III, the averaged shear stress and plastic strain behave in a similar way to those with the transformation in region II; the same is qualitatively true for all the other transforming regions.

An interesting cyclic change in local plastic shear as well as averaged plastic shear occurs at points 4, 6 and 7 and in regions IV and V respectively. In the transformation in region I, the sign of these plastic shears coincides with the sign of the transformation strain. Then, after some stage of elastic straining, plastic shears grow in the opposite direction. The behaviour at point 5 is elastic until transformation starts in region III.

In figure 11 the horizontal displacement distributions along the lines AB, CD and EF shown in figure 2(*d*) are presented. In this way, a fiducial line drawn on the specimen surface is distorted. Along all three lines there is a region with transformation shear inside the martensitic unit, two adjoining regions with plastic shear of the

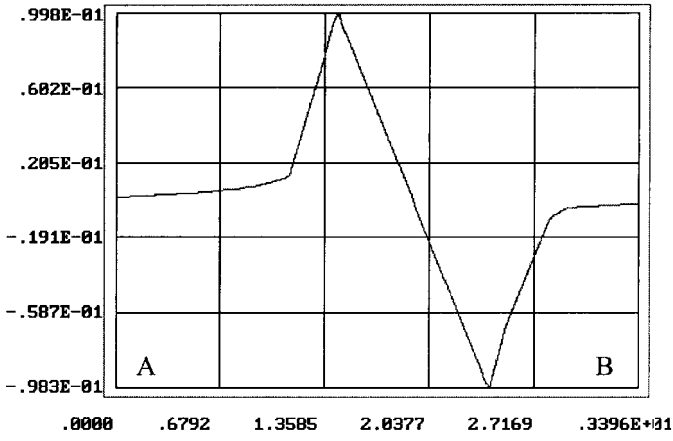

a

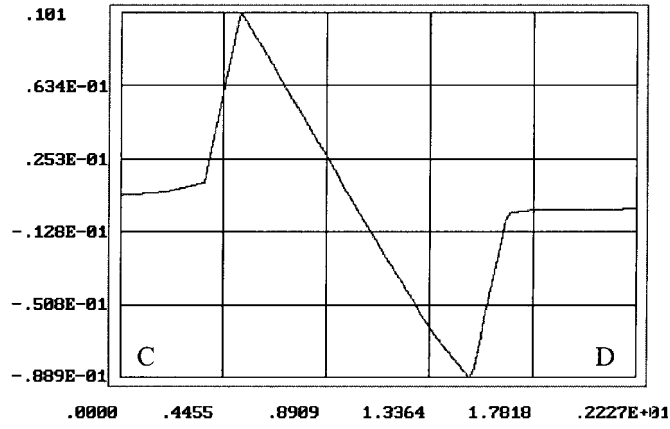

b

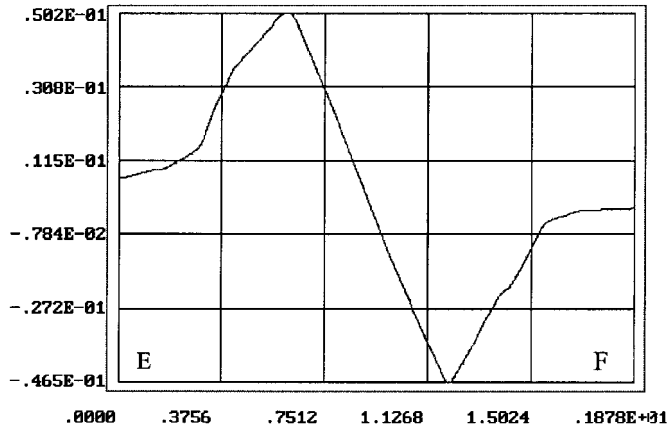

c

Figure 11. Distribution of horizontal displacements along (*a*) line AB, (*b*) line CD and (*c*) line EF, shown in figure 2 (*d*).

same order but with opposite signs and the remaining part which is almost undeformed.

The deformed mesh in the transformed region (figure 2) together with isobands of accumulated plastic strain (figures 3 and 4) allow us to investigate deeper inside the inhomogeneous distribution of shear strains in addition to the information given in figure 10. After PT in region I there is a small region near the short side of the unit in which the plastic strain is very small (figure 3(*a*)) which is in agreement with line 2 and curve 3 in figure 10. The plastic strain is also very small near the martensitic unit after completing the PT in region V (figure 3 (*c*)), which is in agreement with experiments. This related to the relatively small shape change of the contour of the martensitic unit (see the deformed mesh in figure 2). This final picture is observed experimentally and can give the impression that austenite deforms (excluding the narrow zone) elastically and martensite plastically, despite the much higher yield stress of martensite in comparison with austenite. As follows from the transformation process consideration, intense plastic deformations near the interface from the austenite side are inherited by the growing martensite and make a very important contribution to the stress variation and the driving force in the transforming region. The wave-like profile of the martensitic unit after PT in region III (figure 4 (*b*)) is also unexpected; the resulting shear near the corners is directed in the opposite direction to the transformation shear and may be significant for autocatalytic nucleation.

As follows from figure 9, the resisting shear stress in region II during the PT is much higher than in regions IV and V, that is the transformation shear work is smaller in region II than in regions IV and V. At the same time the total transformation work in region II is higher than in regions IV and V (figure 7). This emphasizes the importance of the work of normal stress accompanying transformation dilatation, which is uniquely responsible for the difference.

4.2. *Appearance and growth of martensitic particle near a free surface*

Let us consider the appearance of a martensitic particle close to the free surface of a specimen with its growth crossing the free surface. This is relevant to the problem of surface relief effects associated with displacive transformations. The cross-section of the sample with martensitic unit with designated regions and finite-element mesh before and after transformation is given in figure 12. The initial distance of the particle from the free surface is equal to 1.2 multiplied by the particle thickness. The free surface promotes the plastic accommodation around the growing particle, changes the stress–strain fields and increases the transformation work. After appearance of the martensitic particle and its growth, a plastic hinge between the particle and a free surface appears and grows as well (figure 13). The accumulated plastic strain in the austenite does not exceed 0.452 and is smaller than the maximum value of 0.619 for particle growth in the bulk (figure 3). The deformed mesh (figure 12 (*d*)) illustrates the deformation of the free surface after intersection by a martensitic unit as would be observed in an optical microscope. Plastic deformation in the martensite (figure 14) is also smaller than at the PT in the bulk. The interface profile goes through a wave-like form similar to the martensitic particle in a bulk material (figure 4 (*b*)), but the final form corresponds to transformation shear slightly compensated by plastic accommodation (corresponding to a 'tent-shaped relief') rather than the undeformed profile in the bulk (figure 4 (*c*)). The shear stresses in austenite and martensite are shown in figures 15 and 16 respectively.

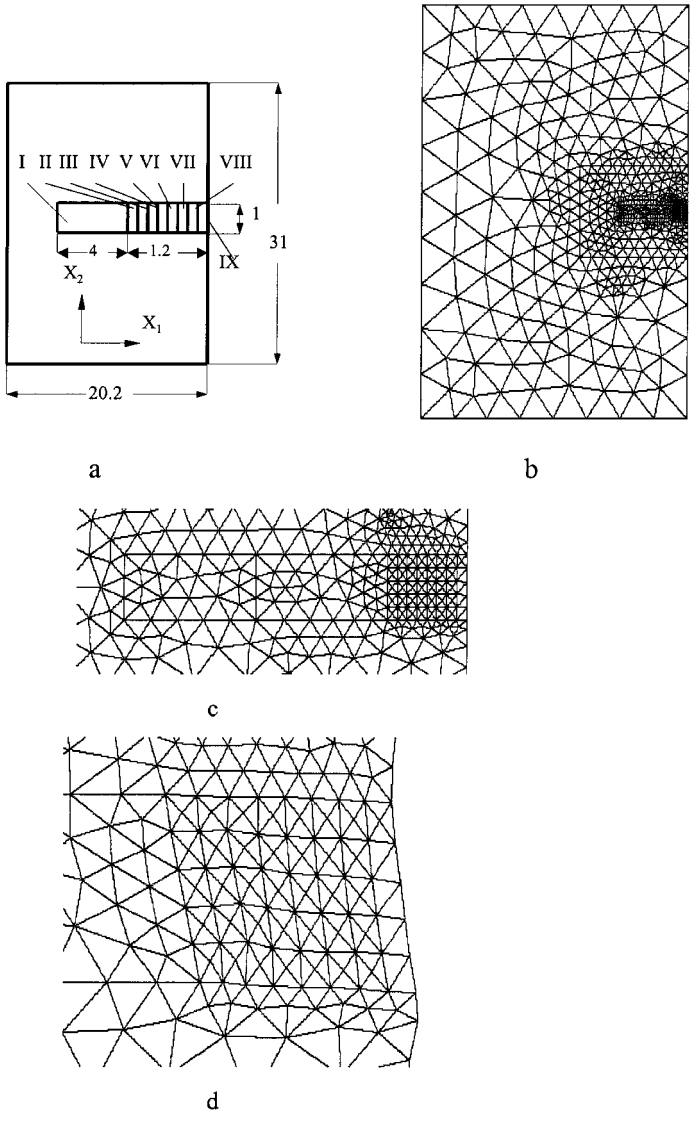

Figure 12. Cross-section of a sample with (*a*) subsequently transforming regions I–IX and (*b*)–(*d*) finite-element mesh before ((*b*) for a whole sample and (*c*) near transforming regions) and after ((*d*) near transformation regions) transformation.

At the appearance of region I the transformation work is $\varphi = -46.4$ MPa (i.e. slightly higher than for a particle far from the free surface); it decreases to -90 MPa during the growth of the region in the l/h range 4.0–4.45 and then increases to -38 MPa in the l/h range 4.45–5.20 owing to the positive effect of the free surface (figure 7). The accumulated plastic strain increases at the first stage and decreases at the second stage. The maximal value of the term $A\bar{q}^{0.5} = 27.78$ MPa corresponds to PT in region IV.

The relationships between the logarithm of the interface velocity and the temperature for the parameters φ and $A\bar{q}^{0.5}$ corresponding to their values in each region

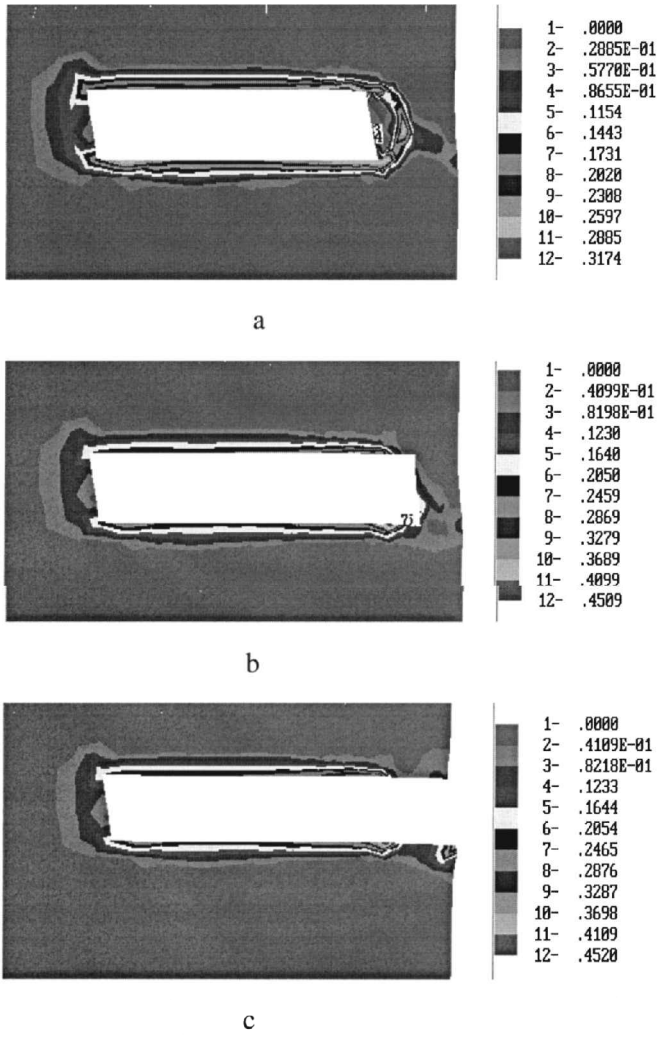

Figure 13. Isobands of the accumulated plastic strains near transformation regions after transformation in (*a*) region I, (*b*) regions I–V and (*c*) regions I–IX.

I–IX, as well as the vertical lines I*–IX* corresponding to fulfilment of the thermodynamic PT criterion are presented in figure 17. The kinetic criterion of interface propagation again corresponds to a detectable interface velocity of the order of $10^{-2}\,\mu\mathrm{m\,s^{-1}}$. If a martensitic region nucleates for example at $\theta = 280\,\mathrm{K}$, at region I the interface propagates with maximum velocity; then the velocity sharply decreases through regions II and III and the interface is arrested before reaching region IV owing to violation of the kinetic (and then thermodynamic) interface propagation criterion, that is the same as for particle growth in bulk material. If the martensitic unit appeared at $\theta = 250\,\mathrm{K}$ or lower, then, after growth with a very high velocity through the regions II and III and sharp deceleration in region IV, the interface accelerates again and after region IV moves with maximum possible velocity to the free surface. In this case a transition from time-dependent, thermally activated

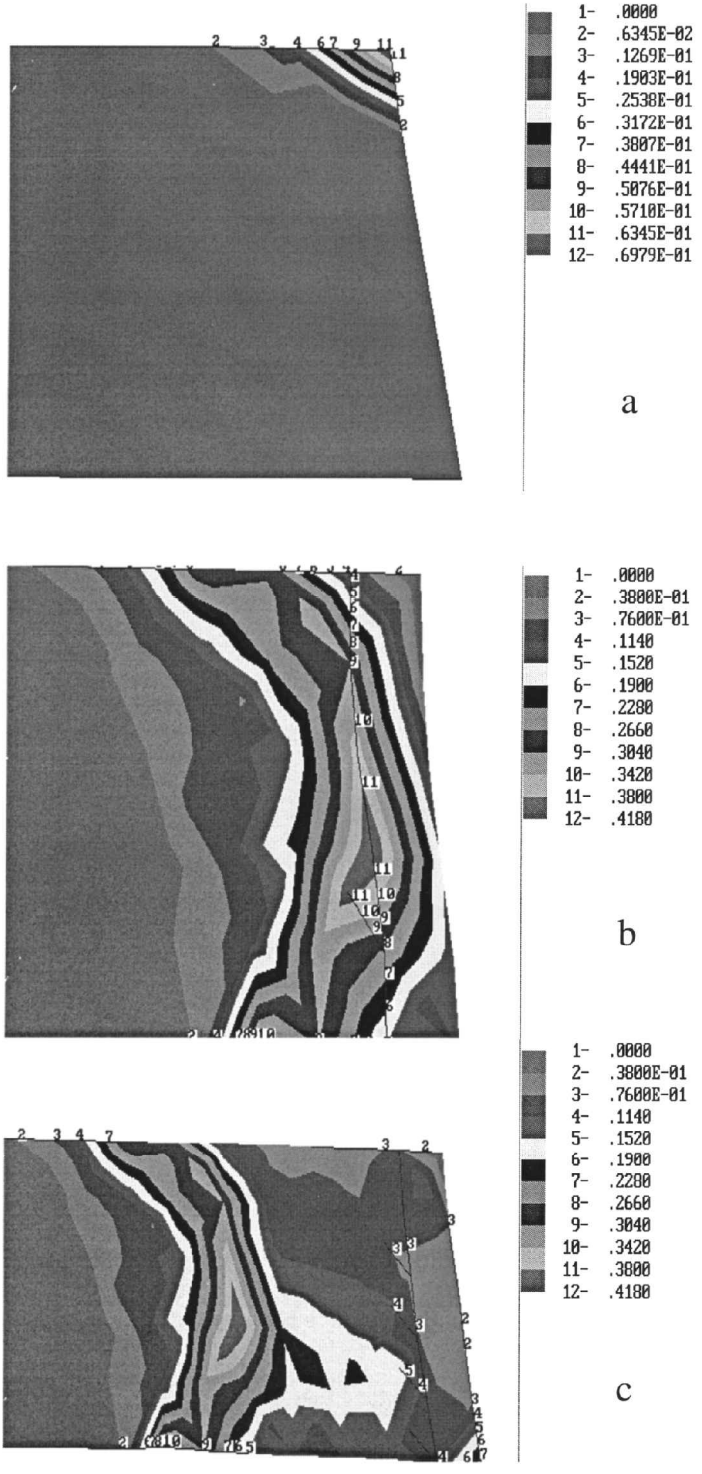

Figure 14. Isobands of the accumulated plastic strains in the right part of the martensitic unit after transformation in (*a*) region I, (*b*) regions I–V and (*c*) regions I–IX.

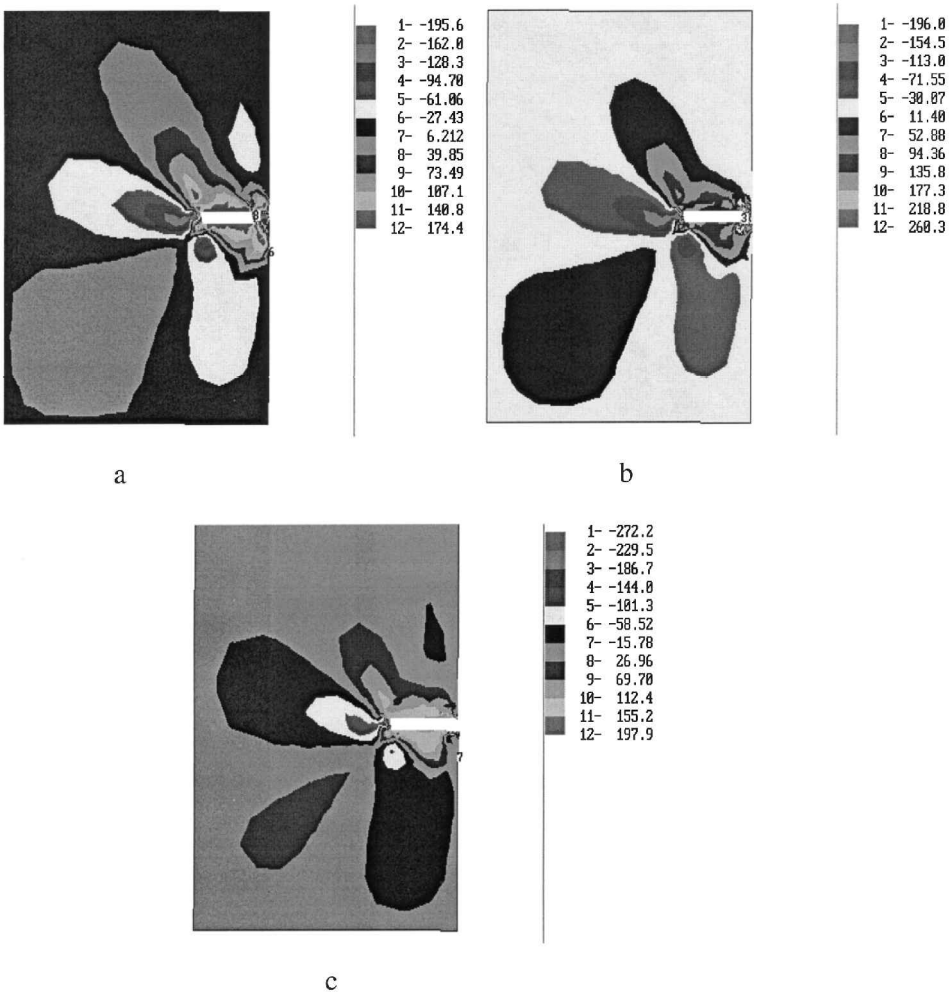

Figure 15. Isobands of shear stress in austenite near transformation regions after transformation in (*a*) region I, (*b*) regions I–V and (*c*) regions I–IX.

kinetics at the interface level to time-independent kinetics at the macrolevel is related to cessation of PT because the free surface is reached, rather than to growth arrest.

Generally, the variation in shear stress and plastic strain averaged over each region designated in figure 12 during the sequential transformation process are very similar to the case without the effect of the free surface. However, some differences can be observed. For example, during the transformation in region I, shear stresses in regions II and III are negative; plastic shear is positive in region II and negative in region III.

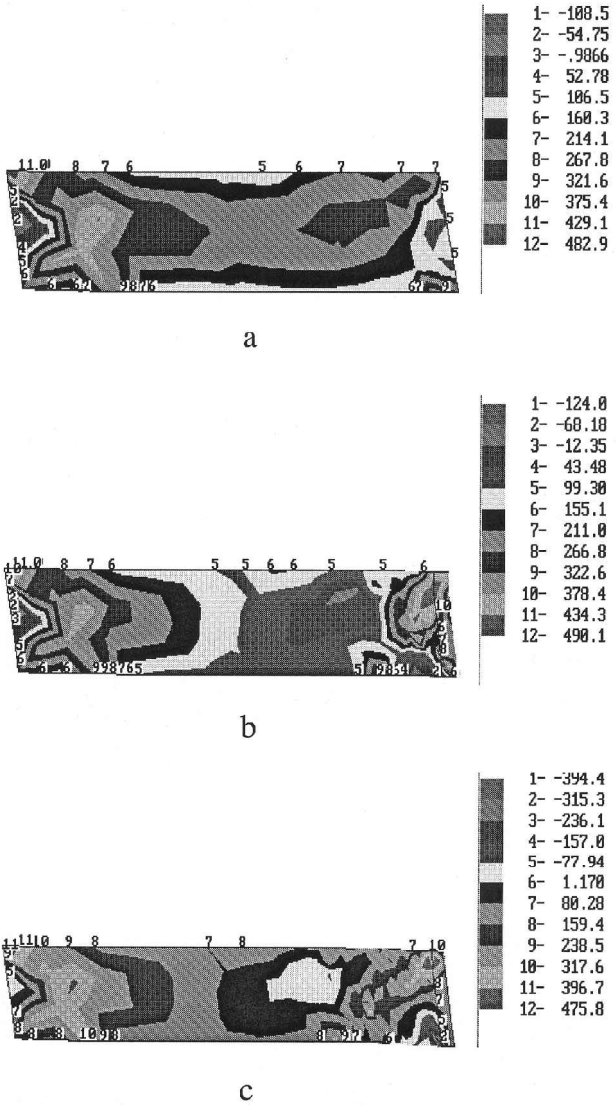

Figure 16. Isobands of shear stress in martensite after transformation in (*a*) region I, (*b*) regions I–V and (*c*) regions I–IX.

4.3. *Step growth*

According to discrete dislocation representations, the interface does not move as a smooth surface, but first a small step or transformation dislocation appears, which then moves along the interface making the PT. This is related to fact that the energy barrier which has to be overcome by thermal fluctuation is proportional to the transforming volume during the activation event (under fixed other parameters); see kinetic equation (A 15) and extremum principle (A 16). The result is a smaller transforming volume, a smaller activation energy and a shorter transformation time. The explicit expression for function F of the kinetic equation has been given in the papers by Levitas (2000) and Idesman *et al.* (2000); however, the use of it together

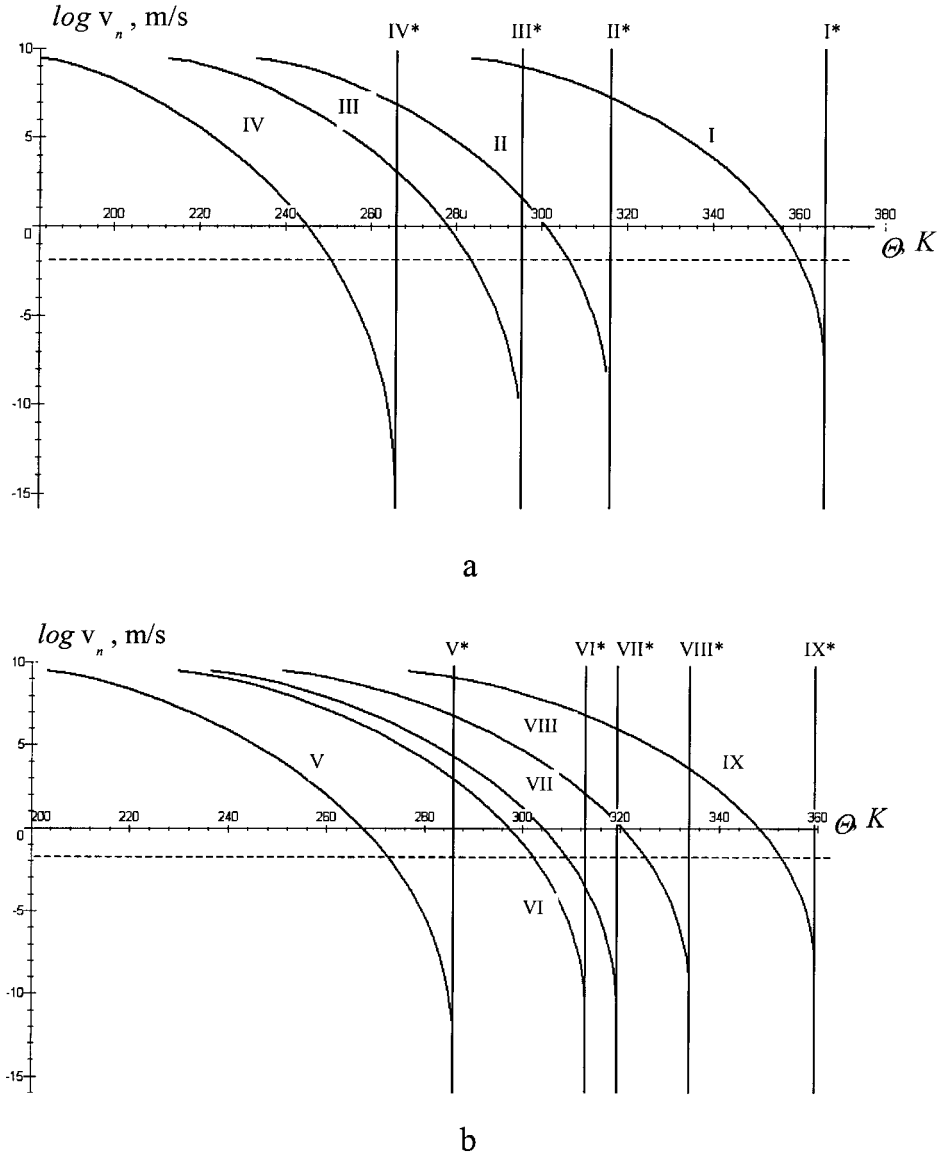

Figure 17. Interface velocity versus temperature for various interface positions (*a*) after PT in regions I–IV and (*b*) after PT in regions V–IX. Curves I, II and IX correspond to the kinetic equation (A 13) after sequential PT in regions I, II and IX respectively. Lines I*–IX* correspond to fulfilment of the thermodynamic PT criterion (A 14) in regions I–IX. The broken line log $v_n = 10^{-2}$ is used for the kinetic PT criterion.

with macroscopic plasticity theory is doubtful. At the same time, as in dissipative materials, everything is history dependent; it makes sense to study semiquantitatively the transformation work at such a mechanism of interface propagation in detail on the mesoscopic level. For this purpose the following problems are solved (figure 18).

Problem 1. After PT in regions I and II with homogeneous growth of transformation strain in these regions, PTs occur

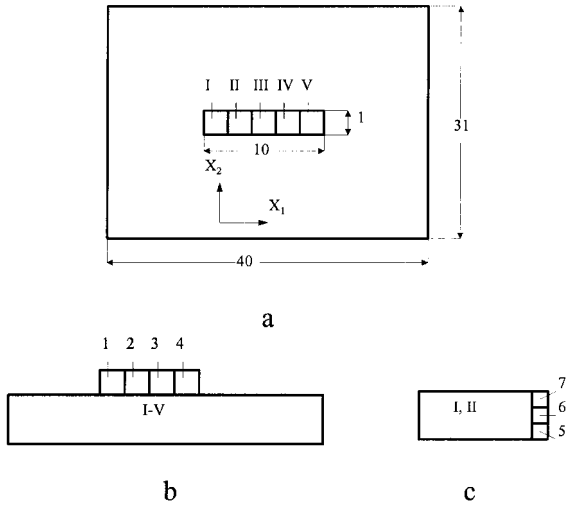

Figure 18. (*a*) Cross-section of a sample used to study the appearance and growth of (*b*) a small longitudinal step and (*c*) a transverse step at the martensitic plate.

(*a*) in a small region 5, then in region 6 and finally in region 7, or
(*b*) in regions 5 and 6, and then in region 7.

Problem 2. After PT in regions I–V with homogeneous growth of transformation strain in these regions, PTs occur

(*a*) in a small region $1 + 2 + 3$, and then region 4, or
(*b*) in regions $1 + 2$, then in region 3 and finally in region 4.

Problem 1 simulates longitudinal step growth, and problem 2 models transverse step growth. The results of calculations of the transformation work for each of these processes are summarized in table 2. Values of the transforming volume at each transformation event are given as well, because $\bar{X}m_n$ is the argument of function F. Analysis of the results shows that the transformation work on the appearance of the first plate is much higher than for its step growth in any direction. For the longitudinal plate growth the amounts of transformation work are approximately the same at PT in regions 5, $5 + 6$ and $5 + 6 + 7$. Allowance for surface energy results in a higher driving force and the first possibility of fulfilment of the thermodynamic PT criterion in the large region $5 + 6 + 7$. If the PT criterion can be fulfilled for each of the transformation processes, the PT will occur in the shortest time in the smallest region 5 rather than in regions $5 + 6$ and $5 + 6 + 7$. Since the transformation work decreases essentially at PT in region 6 after PT in region 5 and especially at PT in region 7 after PT in region $5 + 6$, the growth can be thermodynamically impossible. A small driving force for PT in region 6 and 7 is related to the difficulty of plastic accommodation due to higher yield stress in the surrounding martensite.

Transformation work at plate thickening is slightly smaller for the same transforming volumes than for the longitudinal plate growth. Allowance for heterogeneities in the athermal friction makes the thermodynamic conditions for longitudinal growth and thickening almost equivalent. If, for example, PT starts in region 5 and cannot occur in region 6 or 7 but can occur in region $1 + 2 + 3$ or $1 + 2$, then longitudinal growth will be arrested but thickening will take place.

Table 2. Driving force φ for different scenarios of PTs.

	φ (MPa)	V_n	
PT in I–V	−37.35	10	
PT in 1, 2, 3	−87.44	0.36	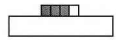
PT in 4 after PT in 1, 2, 3	−88.05	0.12	
PT in 1, 2	−93.03	0.24	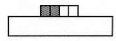
PT in 3 after PT in 1, 2	−91.72	0.12	
PT in 4 after PT in 1, 2, 3	−92.93	0.12	
PT in I, II	−51.32	4	
PT in 5	−84.26	0.12	
PT in 6 after PT in 5	−93.64	0.12	
PT in 7 after PT in 5, 6	−106.74	0.12	
PT in 5, 6	−84.21	0.24	
PT in 5, 6, 7	−85.24	0.36	

The above analysis demonstrates that, in contrast with the elastic case (Olson and Cohen 1986, Haezebrouck 1986), the thermodynamic conditions for the longitudinal growth and thickening of the plate are almost equivalent during plastic growth.

§ 5. Concluding remarks

(1) In this paper a numerical solution of the problem of martensitic growth in an elastoplastic material is considered. It is based on a mesoscopic theory, which combines strict continuum thermodynamic determination for the driving force (Levitas 1998a) with physically based and experimentally verified relations between the driving force and the interface velocity (Olson and Cohen 1986, Ghosh and Olson 1994), and a corresponding numerical method (Idesman *et al.* 1999). Three typical cases are considered: particle growth inside the bulk material, particle growth near the free surface and growth by step motion at the martensitic interface.

(2) Very non-trivial and heterogeneous stress–strain fields in the austenite and martensite and their non-monotonic variation during the transformation process are found. The plastic shear strain at some points can reach 60% in the direction of the transformation shear and, after an elastic stage, change sign and vary by 40%. The edge profile of the moving interface varies in a non-trivial way as well (figure 4); the normal transformation shear profile is followed by a wave-like profile with a reverse shear near the corners, and finally an almost undeformed vertical line. The jump in plastic

shear strain across the interface reaches 90%. These results demonstrate the necessity of a finite-strain treatment and accounting for the jump in plastic strain across the interface in the expression for the driving force. Allowance for the Bauschinger effect, kinematic hardening and crystal plasticity would be desirable in future improved models. It is difficult to reproduce the complex field variations in simplified models for the microscopic-to-macroscopic transition (Cherkaoui *et al.* 1998). However, the good agreement with macroscopic experiments obtained by Cherkaoui *et al.* (1998) suggests that not all these microscopic details are important at the macrolevel.

(3) The solution obtained explains why plastic deformation is concentrated in martensite rather than in austenite, despite the fact that the yield stress of martensite is much larger than the yield stress of austenite. At the initial stage, intense plastic deformations are generated near the interface from the austenite side, which then are inherited by the growing martensite. At further stages, internal stresses cause additional plastic flow in martensite. Plastic flow in austenite is very limited because of relatively a small shape change of the contour of the martensitic unit (see the deformed mesh in figure 2). Such a complex strain variation makes a very important contribution to the driving force and athermal resistance to interface motion.

(4) After appearance of the martensitic particle, the transformation work decreases from -50.35 to -100.79 MPa during lengthening by 10%. The athermal interfacial dislocation forest hardening increases during such growth from zero to 30.22 MPa, which is one order of magnitude higher than the interfacial friction due to solute hardening. Both these changes lead to growth arrest, and consequently to lath martensite instead of plate martensite. At the same time, rather high matrix internal shear stresses can promote autocatalytic nucleation of martensitic variants with the same or opposite transformation shear.

(5) For elastic growth, martensite can be stopped only by a grain boundary or by another martensitic plate only. The growth arrest inside the grain and transition from plate to lath martensite obtained in our calculations is due to interaction of the moving interface with transformation-induced plastic strain. The smaller the yield stress of austenite, the larger is the plastic strain, and the stronger is the tendency to growth arrest. Lath martensite is thus observed for steels with a relatively high martensitic temperature, because the yield stress decreases with increasing temperature. Consequently, by controlling the yield stress of austenite (e.g. by proper alloying), one can control the microstructure and properties of steels.

(6) A free surface does not significantly affect the driving force until its distance from the moving interface falls below $0.75h$. Then the transformation work increases while the accumulated plastic strain q and associated dislocation forest hardening decrease sharply. If the interface is not arrested at this point, it then accelerates to the free surface. The edge interface profile goes through a wave-like form similar to the martensitic region in a bulk material, but the final form corresponds to a transformation shear slightly compensated by plastic accommodation, forming an asymmetric 'tent-shaped' relief.

(7) For time-independent nucleation, the transition from thermally activated kinetics at the interface level to athermal kinetics at the macrolevel is related

to the fact that, independent of interface velocity, growth is terminated after some interface advance owing to violation of the kinetic interface propagation criterion. For growth near the free surface, cessation is due to reaching the free surface.

(8) Analysis of stepwise growth demonstrates that, in contrast with the elastic case (Olson and Cohen 1986, Haezebrouck 1987), the thermodynamic conditions for the longitudinal growth and thickening of the plate are almost equivalent during plastic growth.

In future research, rate and scale effects should be included to better capture path-dependent behaviour in nucleation and growth. This may be based on a combination of dislocation-based viscoplasticity with gradient plasticity.

Acknowledgements

V.I.L. and A.V.I. gratefully acknowledge the support of the Deutsche Forschungsgemeinschaft and Volkswagen Foundation (grant I/70283) and the support of Texas Tech University. Research on martensitic transformation at Northwestern University is sponsored by the National Science Foundation under grant DMR9500122.

APPENDIX A

§ A 1. Problem formulation

A1.1. *Kinematics*

Multiplicative decomposition of the total deformation gradient $\mathbf{F}$ is as follows:

$$\mathbf{F} = \frac{\partial \mathbf{r}}{\partial \mathbf{r}_0} = \mathbf{F}_e \cdot \mathbf{F}_t \cdot \mathbf{F}_p = \mathbf{V}_e \cdot \mathbf{R}_e \cdot \mathbf{F}_t \cdot \mathbf{F}_p. \tag{A 1}$$

The elastic strain tensor $\mathbf{B}_e$ and the dimensionless order parameter ξ are given by

$$\mathbf{B}_e := 0.5(\mathbf{F}_e \cdot \mathbf{F}_e^t - \mathbf{I}) = 0.5(\mathbf{V}_e \cdot \mathbf{V}_e - \mathbf{I}), \quad \xi := \frac{|\mathbf{F}_t - \mathbf{I}|}{|\bar{\mathbf{F}}_t - \mathbf{I}|}. \tag{A 2}$$

The transformation gradient $\mathbf{F}_t$ is

$$\mathbf{F}_t = \mathbf{I} + \xi(\bar{\mathbf{F}}_t - \mathbf{I}), \quad \xi \in [0, 1]. \tag{A 3}$$

Decomposition of the total deformation rate $\mathbf{d}$ is as follows:

$$\mathbf{d} := \left(\frac{\partial \mathbf{v}}{\partial \mathbf{r}}\right)_s = (\dot{\mathbf{F}}_e \cdot \mathbf{F}_e^{-1})_s + \mathbf{d}_t + \mathbf{d}_p, \tag{A 4}$$

where

$$\mathbf{d}_p := (\mathbf{F}_e \cdot \mathbf{F}_t \cdot \dot{\mathbf{F}}_p \cdot \mathbf{F}_p^{-1} \cdot \mathbf{F}_t^{-1} \cdot \mathbf{F}_e^{-1})_s = \mathbf{F}_e \cdot \mathbf{F}_t \cdot \dot{\mathbf{F}}_p \cdot \mathbf{F}_p^{-1} \cdot \mathbf{F}_t^{-1} \cdot \mathbf{F}_e^{-1} \tag{A 5}$$

and

$$\mathbf{d}_t := (\mathbf{F}_e \cdot \dot{\mathbf{F}}_t \cdot \mathbf{F}_t^{-1} \cdot \mathbf{F}_e^{-1})_s = [\mathbf{F}_e \cdot (\bar{\mathbf{F}}_t - \mathbf{I}) \cdot \mathbf{F}_t^{-1} \cdot \mathbf{F}_e^{-1}]_s \dot{\xi}, \quad \dot{q} := (\tfrac{2}{3}\mathbf{d}_p : \mathbf{d}_p)^{1/2}. \tag{A 6}$$

A1.2. *Constitutive equations*

The constitutive equations are as follows: Hooke's elastic law

$$\mathbf{T} = \mathbf{E} : \mathbf{B}_e = KI_1(\mathbf{B}_e)\mathbf{I} + 2G\,\mathrm{dev}\,\mathbf{B}_e, \tag{A 7}$$

the yield function given by

$$f(\mathbf{T}, q, \xi) = \sigma_i - \sigma_y(q, \xi) \leqslant 0, \tag{A 8}$$

and the plastic flow rule

$$\mathbf{d}_p = \lambda \mathbf{s}. \tag{A 9}$$

The loading–unloading conditions are

$$f(\mathbf{T}, q, \xi) \leqslant 0, \quad \lambda \geqslant 0, \quad \lambda f(\mathbf{T}, q, \xi) = 0. \tag{A 10}$$

A1.3. *Equilibrium equation*

The equilibrium is

$$\nabla \cdot \mathbf{T} = 0.$$

A1.4. *Interface propagation*

The interface propagation criterion is

$$\bar{X} \geqslant K_\mu + A\bar{q}^{0.5}, \tag{A 11}$$

where K_μ corresponds to athermal interfacial friction from solution hardening and $A\bar{q}^{0.5}$ corresponds to dislocation forest hardening;

$$\bar{X} := \varphi - \Delta\psi^\theta(\theta), \quad \varphi := \frac{1}{m_n}\int_{V_n}\int_0^1 \mathbf{T} : \mathbf{d}_t \frac{\mathrm{d}t}{\mathrm{d}\xi}\,\mathrm{d}\xi\,\mathrm{d}V_n, \quad \bar{q} := \frac{1}{V_n}\int_{V_n} q_{(\xi=0)}\,\mathrm{d}V_n. \tag{A 12}$$

The kinetic equation for interface propagation is

$$v_n = v_{n0}\exp\left\{-\frac{Q_0}{k\theta}\left[1 - \left(\frac{\varphi - \Delta\psi^\theta - K_\mu - A\bar{q}^{1/2}}{W_0}\right)^p\right]^b\right\}. \tag{A 13}$$

A1.5. *Phase transformation in a transforming region*

The PT criterion is

$$\bar{X} \geqslant K_0, \quad \bar{X} := \varphi - \Delta\psi^\theta(\theta) - \frac{\Delta\Gamma}{m_n}, \tag{A 14}$$

the kinetic equation is

$$t_s = F(X_v, \ldots) = F(\bar{X}m_n, \ldots) \tag{A 15}$$

and the extremum principle for determination of the transforming region V_n^* is

$$t_s = F(\bar{X}^* m_n^*, \ldots) \to \min \quad \text{or} \quad \bar{X}^* m_n^* \to \max. \tag{A 16}$$

References

Cherkaoui, M., Berveiller, M., 2000, *Arch. appl. Mech.*, **70**, 159.
Cherkaoui, M., Berveiller, M., and Sabar, H., 1998, *Int. J. Plasticity*, **14**, 597.

Eshelby, J. D., 1970, *Inelastic Behaviour of Solids,* edited by M. F. Kanninen, W. F. Adler, A. R. Rosenfeld and R. I. Jaffee (New York: McGraw-Hill), pp. 77–115.
Fischer, F. D., Berveiller, M., Tanaka, K., and Oberaigner, E., 1994, *Arch. appl. Mech.*, **64**, 54.
Fischer, F. D., and Reisner, G., 1997, *Acta mater.*, **46**, 2095.
Fischer, F. D., Reisner, G., Werner, E., Tanaka, K., Cailletaud, G., and Antretter, T., 2000, *Int. J. Plasticity*, **16**, 723.
Ganghoffer, J. F., Denis, S., Gautier, E., Simon, A., Simonsson, K., and Sjöström, S., 1991, *J. Phys. IV, C4*, suppl. *III,* **1**, 83.
Ghosh, G., and Olson, G. B., 1994, *Acta metall. mater.*, **42**, 3361, 3371.
Grujicic, M., Olson, G. B., and Owen, W. S., 1985, *Metall Trans.* A, **16**, 1713, 1723, 1735.
Haezebrouck, D. M., 1987, Doctoral thesis, Massachusetts Institute of Technology, Cambridge, Massachusetts.
Idesman, A. V., Levitas, V. I., and Stein, E., 1997, *Comput. Mater. Sci.,* **9**, 64; 1999, *Comput. Met. appl. Mech. Engng,* **173**, 71; 2000, *Int. J. Plasticity,* **16**, 893.
Kaganova, I. M., and Roitburd, A. L., 1987, *Soviet Phys. solid St.,* **29**, 800; 1989, *ibid.,* **31**, 545.
Kochs, U. F., Argon, A. S., and Ashby, M. F., 1975, *Thermodynamics and Kinetics of Slip,* Progress in Materials Science, Vol. 19, edited by B. Chalmers, J. W. Christian and T. B. Massalski. (Oxford: Pergamon).
Kondaurov, V. I., and Nikitin, L. V., 1986, *Mech. Solids,* **21**, 130.
Levitas, V. I., 1997, *J. Mech. Phys. Solids,* **45**, 923, 1203; 1998a, *Int. J. Solids Struct.,* **35**, 889; 1998b, *J. Mech. Phys. Solids,* **46**, 557.
Levitas V. I., 2000, *Int. J. Plasticity,* **16**, 805, 851.
Levitas, V. I., Idesman, A. V., and Olson, G. B., 1999, *Acta mater.,* **47**, 219.
Levitas, V. I., Idesman, A. V., and Stein, E., 1998, *Int. J. Solids Struct.,* **35**, 855.
Marketz, F., and Fischer, F. D., 1994a, *Comput. Mater. Sci.*, **3**, 307; 1994b, *Modelling Simulation Mater. Sci. Engng*., **2**, 1017.
Nishiyama, Z., 1978, *Martensitic Transformation* (New York: Academic Press).
Olson, G. B., and Cohen, M., 1986, *Dislocations in Solids,* Vol. 7, edited by F. R. N. Nabarro (Amsterdam: North-Holland), chapter 37, p. 295.
Patel, J. R., and Cohen, M., 1953, *Acta metall.,* **43**, 531.
Roitburd, A. L., and Temkin, D. E., 1986, *Soviet Phys. solid St.*, **28**, 432.
Simo, J. C., and Miehe, C., 1992, *Comput. Methods Appl. Mech. Engng*., **98**, 41.
Simonsson, K., 1995, Doctoral Thesis 362, Linköping, Sweden.
Wayman, C. M., 1964, *Introduction to the Crystallography of Martensitic Transformation* (London: Macmillan).
Weber, G., and Anand, L., 1990, *Comput. Methods Appl. Mech. Engrg*., **79**, 173.
Wen, Y. H., Denis, S., and Gautier, E., 1999, *Proceedings of the IUTAM Symposium on Micro- and Macrostructural Aspects of Thermoplasticity,* Bochum, Germany, 25–29 August 1997, edited by O. T. Bruhns and E. Stein (Dordrecht: Kluwer), pp. 335–344.